

# Gravitational radiation from gamma-ray bursts as observational opportunities for LIGO and VIRGO

Maurice H.P.M. van Putten<sup>1</sup>, Amir Levinson<sup>2</sup>, Hyun Kyu Lee<sup>3</sup>, Tania Regimbau<sup>1</sup>, Michele Punturo<sup>4</sup>, and Gregory M. Harry<sup>1</sup>

## ABSTRACT

Gamma-ray bursts are believed to originate in core-collapse of massive stars. This produces an active nucleus containing a rapidly rotating Kerr black hole of mass  $M_H$  and angular velocity  $\Omega_H \simeq 1/2M_H$ , surrounded by a uniformly magnetized torus of angular velocity  $\Omega_T = \eta\Omega_H$  represented by two counter-oriented current rings. We quantify black hole-spin interactions with the torus and charged particles along open magnetic flux-tubes subtended by the event horizon at a finite half-opening angle  $\theta_H$ . A major output of  $E_{gw} \simeq 4 \times 10^{53}(\eta/0.1)(M_H/7M_\odot)$  erg is radiated in gravitational waves of frequency  $f_{gw} \simeq 500(\eta/0.1)(7M_\odot/M_H)$  Hz by a quadrupole mass-moment in the torus when its minor-to-major radius is less than 0.3260. The durations correspond to the lifetime  $T_s$  of black hole-spin, determined by a stability condition of poloidal magnetic field energy-to-kinetic energy  $< 1/15$  in the torus. Consistent with GRB-SNe, we find (i)  $T_s \simeq 90$ s (tens of s, Kouveliotou et al. 1993), (ii) aspherical SNe of kinetic energy  $E_{SN} \simeq 2 \times 10^{51}$ erg ( $2 \times 10^{51}$ erg in SN1998bw, Höflich et al. 1999) and (iii) GRB-energies  $E_\gamma \simeq 2 \times 10^{50}$ erg ( $3 \times 10^{50}$ erg in Frail et al. 2001), upon associating  $\theta_H$  with poloidal curvature of the magnetosphere. GRB-SNe occur perhaps about once a year within  $D = 100$ Mpc. Correlating LIGO/Virgo detectors enables searches for nearby events and their spectral closure density  $6 \times 10^{-9}$  around 250Hz in the stochastic background radiation in gravitational waves. At current sensitivity, LIGO-Hanford may place an upper bound around  $150M_\odot$  in GRB030329. Upcoming all-sky supernovae surveys may provide distances to GRB-SNe, conceivably coincident with weak wide-angle GRB emissions similar to the nearby event GRB980425/SN1998bw. Detection of  $E_{gw}$  thus provides a method for identifying Kerr black holes by calorimetry.

---

<sup>1</sup>LIGO Laboratory, NW17-161, 175 Albany Street, Cambridge, MA 02139-4307, USA

<sup>2</sup>School of Physics and Astronomy, Tel Aviv University, 69978 Tel Aviv, Israel, and School of Physics, University of Sydney, NSW2006, Australia

<sup>3</sup>Department of Physics, Hanyang University 133-791, Seoul, and APCTP, Pohang, 790-784, Korea

<sup>4</sup>Virgo Project, Istituto Nazionale di Fisica Nucleare, Sezione di Perugia, Perugia, Italy

## 1. Introduction

Gravitational wave detectors LIGO (Abramovici et al. 1992) and Virgo (Bradaschia et al. 1992), are broad-band detectors, most sensitive in 20-1000 Hz. They introduce new opportunities for probing strongly-gravitating astrophysical sources and the stochastic background radiation in gravitational waves – see (Cutler & Thorne 2002) for a recent overview. Notable candidates for burst sources of gravitational radiation are binary coalescence of neutron stars and black holes (Narayan, Piran & Shemi 1991; Phinney 1991), newborn neutron stars (Ferrari et al. 2003), and gamma-ray bursts: long bursts associated with supernovae (van Putten 2001; Mészáros 2002; van Putten & Levinson 2003) and short bursts, conceivably associated with black hole-neutron star coalescence. Collectively, these astrophysical sources may contribute appreciably to the stochastic background in gravitational waves. Of particular interest is the quest for identifying Kerr black holes in the Universe, and these objects may be at the center of cosmological GRBs.

The events GRB980425/SN1998bw (Galama et al. 1998) and GRB030329 (Hjorth et al. 2003; Stanek et al. 2003) demonstrate that long GRBs are associated with Type Ic supernovae. This provides considerable support for GRBs as core-collapse events in massive stars in binaries (Woosley 1993; Paczynski 1998; Brown et al. 2000), and hence an association with star-forming regions. A correlation of the current flux-limited sample of 33 GRBs with individually measured redshifts with the cosmic star formation rate shows a true-to-observed GRB event rate of 450 (van Putten & Regimbau 2003), which is very similar to the beaming factor of 500 obtained from a subsample of GRBs with achromatic breaks in their light curves (Frail et al. 2001). The true GRB-event rate is hereby about one per year within a distance of 100Mpc. The associated supernova and late-time GRB-afterglows may present wide-angle optical and radio emissions as orphan transients to nearby events. Because the event rate of GRB980425/SN1998bw is roughly consistent with the true GRB-event rate, nearby events are conceivably detectable by extremely weak but non-vanishing GRB emissions at large viewing angles.

Here, we report on signal-to-noise ratios for gravitational radiation from GRBs from rotating black holes in matched filtering and in correlating two detectors of LIGO and Virgo, both in targeting GRBs as nearby point sources and in their contribution to the stochastic background radiation. Detection of these emissions from GRBs with measured redshifts enables calorimetry on their inner engines, as a method for rigorously identifying Kerr black holes as objects in the Universe.

We propose a radically new model (Fig. 1): GRB-SNe produced by an active nucleus in a remnant stellar envelope comprising a Kerr black hole, surrounded by a uniformly magnetized torus in suspended accretion represented by two counter-oriented current rings

(van Putten 1999; van Putten & Ostriker 2001; van Putten 2001; van Putten & Levinson 2002, 2003). Our model predicts an energetic output in gravitational waves from black hole-spin energy with energy output and frequency

$$E_{gw} \simeq 0.2M_{\odot} \left( \frac{\eta}{0.1} \right) \left( \frac{M_H}{7M_{\odot}} \right), \quad f_{gw} \simeq 500\text{Hz} \left( \frac{\eta}{0.1} \right) \left( \frac{7M_{\odot}}{M_H} \right) \quad (1)$$

emitted by a non-axisymmetric torus surrounding the black hole. Here, we measure energy in units of  $M_{\odot} = 2 \times 10^{54}\text{erg}$ , and  $\eta$  denotes the ratio of the angular velocity of the torus to that of the black hole of mass  $M_H$ , which represents the efficiency of converting black hole-spin energy into radiation by the torus. Because the system is relativistically compact, most of the torus output is in gravitational radiation by multipole mass-moments (van Putten 2001). It has not eluded us, that the output in gravitational radiation (1) surpasses  $E_{\gamma} \simeq 3 \times 10^{50}\text{erg}$  in gamma-rays (Frail et al. 2001) by three orders of magnitude.

A quadrupole mass-moment associated with a mass-inhomogeneity  $\delta M_T$  produces a luminosity (Peters & Mathews 1963)

$$L_{gw} = \frac{32}{5} (\omega \mathcal{M})^{10/3} F(e) \simeq \frac{32}{5} (M_H/R)^5 (\delta M_T/M_H)^2, \quad (2)$$

where  $\omega \simeq M^{1/2}/R^{3/2}$  denotes the orbital frequency of the torus with major radius  $R$ ,  $\mathcal{M} = (\delta M_T M_H)^{3/5}/(\delta M_T + M_H)^{1/5} \simeq M_H (\delta M_T/M_H)^{5/3}$  denotes the chirp mass, and  $F(e)$  denotes a geometric factor representing the ellipticity  $e$  of the orbital motion. Application of (2) to PSR1913+16 with ellipticity  $e = 0.62$  (Hulse & Taylor 1975) provided the first evidence for gravitational radiation consistent with the linearized equations of general relativity to within 0.1% (Taylor 1994). Here, we apply the right hand-side of (2) to a non-axisymmetric torus around a black hole, whose mass-quadrupole inhomogeneity  $\delta M_T$  is determined self-consistently in a state of suspended accretion for the lifetime of rapid spin of the black hole. A quadrupole mass-moment appears spontaneously as a Papaloizou-Pringle wave (Papaloizou & Pringle 1984) whenever the torus is sufficiently slender, i.e., for a ratio  $b/R < 0.3260$ , where  $b$  denotes the minor radius of the torus (van Putten 2002). In the suspended accretion state, most of the black hole-spin energy is dissipated in the event horizon for typical ratios  $\eta \sim 0.1$  of the angular velocity of the torus to that of the black hole. Hence, the lifetime of rapid spin of the black hole is effectively determined by the rate of dissipation of black hole-spin energy in the event horizon, itself bounded by a finite ratio  $\mathcal{E}_B/\mathcal{E}_k < 1/15$  of the poloidal magnetic field energy-to-kinetic energy in the torus (van Putten & Levinson 2003). This gives rise to long durations of tens of seconds for the lifetime of rapid spin of the black hole. The resulting gravitational wave-emissions should be limited in band width, changing in frequency about 10% during the emission of the first 50% of its energy output. This change mirrors a decrease of 10% in the angular velocity of a maximally-spinning black hole

in converting 50% of its spin-energy. Thus, gravitational radiation is connected to Kerr black holes, representing a connection between the linearized equations of general relativity and, respectively, fundamental objects predicted by the fully nonlinear equations of general relativity.

To date, short GRBs appear to have featureless afterglow emissions, and their cosmological origin is based on an isotropic distribution in the sky and a  $\langle V/V_{max} \rangle = 0.385 \pm 0.019$  distinctly less than 1/2 (Katz & Canel 1996). These events are probably disconnected from star-forming regions, and may be produced by black hole-neutron star-coalescence (Paczynski 1998), possibly associated with hyperaccretion onto slowly-rotating black holes (van Putten & Ostriker 2001). While the wave-form of binary inspiral is well-understood up to 3.5 post-Newtonian order (see Cutler & Thorne (2002)), gravitational wave-emissions from the coalescence and merger of a neutron star onto a slowly-rotating black hole is highly uncertain. Depending on the black hole mass and spin, the neutron star may break up by tidal forces outside the innermost stable circular orbit, and subsequently form a torus which merges with the black hole. A torus formed from the debris of a neutron star outside the ISCO of a stellar mass black hole should be unstable. Quite generally, non-axisymmetries may develop as Papaloizou-Pringle waves (Papaloizou & Pringle 1984) in tori of finite slenderness (see van Putten & Levinson (2003)). In case of a massive torus formed from the debris of a neutron star, self-gravity may also excite non-axisymmetric instabilities. Gravitational radiation emitted in the inspiral phase is about  $0.2M_{\odot}$ , followed by the emission of conceivably  $0.1M_{\odot}$  during the merger phase with the black hole. This suggests that short GRBs are potentially as energetic in their gravitational wave-emissions as long bursts.

Gravitational radiation associated with collapsars has been considered in a number of other studies (Nakamura & Fukugita 1989; Mönchmeyer et al. 1991; Bonnel & Pringle 1994; Davies et al. 2002; Fryer et al. 2002; Mineshige et al. 2002; Kobayashi & Meszaros 2002), also in model-independent search strategies associated with GRBs (Finn, Mohanty & Romano 1999; Modestino & Moleti 2002). These studies focus on gravitational radiation produced by the release of gravitational binding energy during collapse and in accretion processes on a newly formed black hole (e.g, Fryer et al. (2001)). We note that accretion flows are believed to be strongly turbulent, which may imply a broad spectrum of gravitational radiation. Forementioned studies on gravitational radiation in core-collapse of a massive star do not invoke the spin-energy of a newly formed black hole. They appear to indicate an energy output, which leaves a range of detectability by current ground based detectors of up to about 10Mpc. These events should therefore be considered in the context of core-collapse events independent of the GRB phenomenon, in light of current estimates on the local GRB event rate as referred to above. Currently published bounds on gravitational wave emissions from GRBs are provided by bar detectors (Tricarico et al. 2001; Astone et al. 2002). These

studies and results are important in identifying various detection strategies and channels for producing gravitational waves. We suggest that the design of optimal detection strategies for gravitational radiation from GRBs may be facilitated by a priori knowledge from a specific model.

In the presented studies, we describe a model for GRB-SNe from rotating black holes which is consistent with the observed durations and true energies in gamma-rays from magnetized baryon-poor jets subtended by the event horizon of a black hole (1), the observed total kinetic energies in an associated supernova, possibly radio loud, with aspherical distribution of high velocity ejecta (2), and X-ray line-emissions produced by underlying continuum emissions (3). On this basis, we predict band-limited gravitational wave line-emissions contemporaneous with the GRB according to the scaling relations (1) at an event rate of probably once a year within a distance of 100Mpc.

In §2, we describe elements of current GRB-phenomenology. In §3-4 we summarize a theory of GRB-supernovae from rotating black holes. In §5, we discuss line-broadening in response to Lense-Thirring precession. A semi-analytical estimate is given of the contribution to the stochastic background in gravitational waves in §6. In §7, we present the dimensionless characteristic strain-amplitudes, and in §8 we calculate the signal-to-noise ratios in advanced LIGO and Virgo operations in various detection strategies. §8 introduces a proposed detection strategy for time-frequency trajectories of slowly varying line-emissions. We summarize our findings in §10.

## 2. Phenomenology of GRB-supernovae

X-ray localization of GRBs by BeppoSax introduced the post-BATSE development of providing a sample of GRBs with individually measured redshifts (Table 1). The recent HETE-II burst GRB 030329 has greatly enhanced our confidence in a GRB association to Type Ib/c supernovae, based on a similarity of its optical light curve and emission-lines to that of SN1998bw (Hjorth et al. 2003; Stanek et al. 2003). This observational association supports a GRB event rate which is locked to the star-formation rate, as core-collapse events in evolved massive stars (Woosley 1993; Paczynski 1998; Brown et al. 2000). This is consistent with recent statistical correlations over a broad range of redshifts (Scheafer et al. 2001). It appears that Type Ib/c SNe occur only in spiral galaxies (Cappellaro et al. 1997). Further evidence for the GRB-supernova association is found in X-ray line-emissions in GRB970508 (Piro et al. 1999), GRB970828 (Yoshida et al. 1999), GRB991216 (Piro et al. 2000), GRB000214 (Antonelli et al. 2000) and GRB011211 (Reeves et al. 2001).

When attributing the X-ray line-emissions to excitation by high-energy continuum emissions with energy  $E_r$ , Ghisellini et al. (2002), based on Lazzati et al. (2002), estimate substantial lower bounds for  $E_r$ : long-lived iron-line emissions in GRB99126 may require  $E_r \geq 4 \times 10^{52}$  erg, whilst lines from lighter elements in GRB011211 may likewise require  $E_r \geq 4.4 \times 10^{51}$ . These lower bounds point towards an energy reservoir in excess of that required for the true GRB-energies  $E_\gamma$ . We interpret this as support for the notion that GRB inner engines may be processing other channels, which are contemporaneous with the baryon-poor input to the GRB-afterglow emissions.

The discovery of achromatic breaks in the light curves of some of these GRBs allowed the determination of the true GRB-energies of about  $3 \times 10^{50}$  erg, upon correcting the isotropic equivalent emissions by an observed beaming factor of about 500 (Frail et al. 2001). The redshift distribution of the flux-limited sample of 33 GRBs, locked to the SFR, allows us to estimate the unseen-to-observed GRB rate to be about 450 based on a log-normal fit of the peak-luminosity function – see Fig. 2 (van Putten & Regimbau 2003). This result is very similar to the observed beaming factor of 500. With the ratio 450 of the unseen-to-observed GRBs, the true-but-unseen GRB event rate to about  $0.5 \times 10^6$  per year or, equivalently, 1 per year within a distance of 100Mpc. This event rate agrees with that based on a fraction of about 1% of SNe Ib/c that might be associated with GRBs (Salmonson 2001). Note that our event rate is a lower bound on the rate of formation of GRB inner engines, since we are seeing only those events in which the remnant stellar envelope is successfully penetrated by a baryon poor jet, e.g., when the jet is sufficiently collimated. The true rate of formation of GRB inner engines is therefore an important open question.

The relatively narrow distribution of GRB-energies around  $3 \times 10^{50}$  erg is indicative of a standard energy reservoir (Frail et al. 2001). An anticorrelation between the observed opening angle and redshift points towards wide-angle GRB emissions which are extremely weak, as in GRB980425. Given that the event rate of GRB980425 at  $D = 34$  Mpc is roughly consistent with 1 per year within  $D = 100$  Mpc, these wide-angle emissions may also be standard. Thus, we are led to consider strongly anisotropic GRB emissions in response to outflow in two directions along the rotational axis of the progenitor star, accompanied by extremely weak GRB emissions in all directions (see further Eichler & Levinson (1999); Zhang & Meszaros (2002); Rossi et al. (2002)). In this regard, GRB980425 ( $E_{\gamma,iso} \simeq 10^{48}$  erg,  $z = 0.0085$ ) is *not* anomalous, and GRB030329 ( $E_\gamma \simeq 3 \times 10^{49}$  erg,  $z = 0.167$ ) is intermediate (Price et al. 2003). GRBs may be geometrically standard, in that this anisotropy is similar in its angular distribution in all sources. In this event, the inferred beaming factor depends on redshift, i.e., is a function of the flux-limit in the sample at hand. Current GRB samples with individually measured redshifts, including that of Frail et al. (2001), are dominated by sources with redshifts around unity.

Recent detection of linear polarization GRB021206 provides evidence of synchrotron radiation in magnetized outflows, which may indicate large-scale magnetic fields of or produced by the inner engine (Coburn & Boggs 2003). Afterglow emissions to GRB030329 include optical emissions (Price et al. 2003) with intraday deviations from powerlaw behavior (Uemura et al. 2003), possibly reflecting an inhomogeneous circumburst medium or latent activity of the inner engine (Chevalier & Li 1999; Price et al. 2003).

Furthermore, Type Ib/c SNe tend to be radio-loud (Turatto 2003), as in SN1990B (van Dyk et al. 1993). This includes GRB980425/SN1998bw (Kulkarni et al. 1998; Iwamoto 1999) as the brightest Type Ib/c radio SN at a very early stage (Weiler et al. 2001). GRB030329 might also feature some radio emission associated with the associated SN2003dh (Willingale et al. 2003). Radio emissions in these SNe are well described by optically thick (at early times) and optically thin (at late times) synchrotron radiation of shells expanding into a circumburst medium of stellar winds from the progenitor star (Li & Chevalier 1999). All core-collapse SNe are strongly non-spherical (Höflich et al. 2001), as in the Type II SN1987A (Höflich 1991) and in the Type Ic SN1998bw (Höflich et al. 1999), based, in part, on polarization measurements and direct observations. Observed is a rotational symmetry with axis ratios of 2 to 3. This generally reflects the presence of rotation in the progenitor star and/or in the agent driving the explosion. Aforementioned X-ray line-emissions in GRB011211 may be excited by high-energy continuum emissions of much larger energies (Ghisellini et al. 2002). For Type Ib/c supernovae association with a GRB, these considerations have led some to suggest the presence of new explosion mechanism (Woosley et al. 1999).

Ultimately, GRB-supernova remnants take the form of a black hole in a binary with an optical companion, surrounded by a supernova remnant (van Putten & Levinson 2003). This morphology is illustrated by RX J050736-6847.8 (Chu et al. 2000), if its X-ray binary harbors a black hole. The accreting binary may hereby appear as a soft X-ray transient in the scenario of Brown et al. (2000).

### 3. GRB-supernovae from rotating black holes

GRBs are believed to be produced in core-collapse of massive stars (Woosley 1993), whose angular momentum most likely derives from orbital angular momentum during a common envelope stage (Paczynski 1998). The common envelope stage must ensue only when the progenitor star is evolved (Brown et al. 2000). Core-collapse in this scenario describes an initial implosion which produces an active nucleus consisting of a Kerr black hole surrounded by a magnetized torus, inside a remnant stellar envelope. Evidently, the black hole-torus system is relativistically compact, in that its linear size is on the order of its

Schwarzschild radius. The nucleus is active, by virtue of the spin-energy of the black hole, as outlined below.

### 3.1. MeV nuclei in a remnant envelope

We consider a uniformly magnetized torus around a rapidly rotating black hole in its lowest energy state. This introduces radiative processes through two spin-interactions with the black hole: a spin-connection to the torus and a spin-orbit coupling to charged particles along open magnetic flux-tubes. The torus hereby catalyzes black hole-spin energy into gravitational radiation, accompanied by winds, thermal and MeV-neutrino emissions. The open magnetic flux-tubes produce baryon poor outflows and subsequent high-energy radiation. This result is a broad range of emissions. In what follows,  $\Omega_H$  denotes the angular velocity of the black hole and  $\Omega_T$  denotes the angular velocity of the torus.

A uniformly magnetized torus introduces an ordered poloidal magnetic flux, represented by two counter-oriented current rings. The equilibrium moment of the black hole preserves essentially uniform and maximal horizon flux. When viewed in poloidal cross-section, the inner and the outer torus magnetosphere are topologically equivalent to that of a rapidly rotating neutron star with angular velocities  $-(\Omega_H - \Omega_T)$  and  $\Omega_T$ , respectively. The interface between the inner and the outer torus magnetospheres is an ellipsoidal separatrix (Fig. 3). An open magnetic flux-tube subtended by the event horizon of the black hole may form by moving the separatrix of the inner and outer torus magnetosphere to infinity (van Putten & Levinson 2003). We emphasize that the equivalence between the inner face of the torus and a pulsar is exact in topology, yet refers to similar but not identical physical states. For example: there exist corresponding annuli of  $B = 0$  between the last closed field-lines of the torus and the event horizon, and between the last closed field-lines of the pulsar and infinity, where the former features a spark gap which is absent in the latter; both the event horizon and asymptotic infinity are null-surfaces, where the former but not the latter is endowed with finite surface gravity and the no-hair theorem.

Equivalently to pulsars, the inner face of the torus emits negative angular momentum Alfvén waves into the event horizon, while the outer face emits positive angular momentum Alfvén waves to infinity. Both emissions satisfy causality. The torus hereby develops a state of suspended accretion, described by balance of energy and angular momentum flux received by the spin-connection to the black hole and emitted in various channels. In response to this catalytic process, the black hole evolves by conservation of energy and angular momentum consistent with the no-hair theorem. While most of the spin-energy is dissipated in the event horizon of the black hole, most of the black hole-luminosity is incident onto the inner face of



the torus. The latter represents substantial fraction of black hole-spin energy, given by the ratio of the angular velocity of the torus to that of the black hole, and is mostly reradiated into gravitational radiation by multipole mass moments in the torus. Dominant emissions in gravitational radiation are typical for systems whose linear size is on the order of their Schwarzschild radius, and similar to those from new born neutron stars (Shapiro & Teukolsky 1983). The catalytic emissions by the torus last for the lifetime of rapid spin of the black hole. Contemporaneously, the torus radiates a minor output in baryon-rich magnetic winds, thermal and MeV-neutrino emissions. The remnant stellar envelope is hereby irradiated from *within* by high-energy radiation coming off the torus winds. This associated outgoing radial momentum drives a non-spherical supernova with subsequently X-ray line-emissions when the expanding envelope reaches optical depth of unity or less. Ultimately, this leaves a supernova remnant around a black hole in a binary with an optical companion.

A spin-orbit coupling between the black hole and charged particles creates charged outflows along open magnetic flux-tubes subtended by the event horizon of the black hole. Moving the separatrix in Fig. 3 to infinity by a stretch-fold-cut creates these open flux-tubes with a finite opening angle on the horizon (Fig 10 in van Putten & Levinson (2003)). In the lowest energy state of the black hole, the spin-orbit coupling introduces the identity (Hawking 1976; van Putten 2000)

$$e\text{EMF}_\nu = \nu\Omega_H \quad (\text{in eV}) \quad (3)$$

on charged particles of angular momentum  $\nu = eA_\phi$  in their Landau states along magnetic flux-surfaces  $A_\phi = \text{const.}$ , where  $2\pi A_\phi$  denotes the magnetic flux and  $-e$  the charge of the electron. This coupling enables the black hole to convert mechanical work by rotation into electrical currents *along* the axis of rotation. Mediated by frame-dragging, this process is causal and local in origin, in that it corresponds to the line-integral of the electric field along the magnetic field in Wald (1974). It may be compared with currents induced by Lorentz forces on charged particles when forced to cross magnetic field-lines, with the remarkable distinction that the former produces an EMF parallel to and the latter produces an EMF orthogonal to magnetic field-lines. The net current along the open flux-tube is determined by the detailed state of the magnetosphere formed by charge-separation and the boundary conditions on the horizon and at infinity, as discussed in van Putten & Levinson (2003). In response to the induced charged outflows, the black hole evolves by conservation of energy, angular momentum and charge consistent with the no-hair theorem and, if present, current closure. The fraction of black hole-spin energy released in baryon-poor outflows along open magnetic flux-tubes tends to be small for a finite horizon half-opening angle on the horizon. The outflows consist primarily of  $\gamma e^\pm$ , Poynting flux and kinetic energy in baryonic contaminants. We associate these emissions with the baryon-poor input to GRBs. These represent dissipation of kinetic energy according to the internal shock model (Rees & Mészáros 1994;

Piran 1999; Mészáros 2002). Note that the true energy  $E_\gamma \simeq 3 \times 10^{50}$  (Frail et al. 2001) in gamma-rays represents a mere 0.01% of the rotational energy of a stellar mass black hole. The magnetized baryon-poor outflows are surrounded by magnetized baryon-rich winds coming off the torus. The latter may provide collimation to the former (Levinson & Eichler 2000). Scattering of photons onto the boundary layer between the two produces highly polarized radiation, which may exceed that attainable in synchrotron emissions within the collimated baryon-poor jet (Eichler & Levinson 2003).

Our model is parametrized as follows. The nucleus contains a black hole of mass  $M_H$ , angular momentum  $J_H = aM_H$  and electric charge  $q$ , where  $a/M_H = \sin \lambda$  denotes the specific angular momentum. Because all particles approaching the event horizon assume the angular velocity  $\Omega_H = \tan(\lambda/2)/2M_H$ , there is a magnetic moment  $\mu_H = qa$  aligned with its axis of rotation (Carter 1968). It preserves essentially uniform and maximal horizon flux at arbitrary rotation rates in equilibrium with a surrounding torus magnetosphere of field-strength  $B$  with  $\mu_H \simeq 2BM_H r_H^2$ , where  $r_H = 2M_H \cos^2(\lambda/2)$  denotes the radius of the event horizon (van Putten 2001). Upon balance with various radiation channels, the torus develops a state of suspended accretion at MeV temperatures in equilibrium with its input in energy and angular momentum through the spin-connection to the central black hole. The fractions of black hole-spin energy radiated into various channels depend on the angular velocity  $\eta$  of the torus relative to that of the black hole, the slenderness  $\delta = b/2R$  of the torus in terms of one-half the ratio of the minor radius  $b$  to the major radius  $R$ , and the mass-fraction  $\mu = M_T/M_H$  of the torus mass  $M_T$  relative to  $M_H$ . The half-opening angle of the open magnetic flux-tube on the event horizon of the black hole is denoted by  $\theta_H$ .

In the suspended accretion state, the torus assumes a state of differential rotation which exceeds that of Keplerian motion. The inner face is super-Keplerian, while the outer face is sub-Keplerian due to competing surface stresses on the inner face and the outer face of the torus by, respectively, the action of the black hole and torus winds to infinity. Both faces may develop surface waves, similar to water waves in channels of finite depth, since the effective gravity is outgoing in the inner face and ingoing on the outer face. In the corotating frame, the inner and outer faces may carry retrograde, respectively prograde waves. This allows the former to decrease its angular momentum and the latter to increase it angular momentum. Any coupling between these the inner and outer surface waves would lead to angular momentum transfer from the inner to the outer face, which may result in instability. This picture describes the Papaloizou-Pringle waves (Papaloizou & Pringle 1984), originally discovered as an azimuthal symmetry breaking instability in tori of infinite slenderness ( $b/R \rightarrow 0$ ). An extension of this theory to tori of finite slenderness ( $b/R = 0 - 1$ ) shows that the  $m \neq 0$  wave-modes become successively unstable as the torus becomes more

slender. We have (van Putten 2002)

$$b/R < 0.7506, 0.3260, 0.2037, 0.1473, 0.1152, \dots, 0.56/m, \quad (4)$$

for the onset of instability of the  $m$ -th buckling mode at the point of Rayleigh stability (stability of the  $m = 0$  mode between the two faces). In the proposed suspended accretion state, the amplitude of the resulting quadrupole mass-moment, possibly accompanied by higher order mass-moments, saturates in energy and angular momentum balance between input from the black hole and output in forementioned radiation channels. These hydrodynamic instabilities may be accompanied by other instabilities, such as those associated with a strong magnetic field. The strength of the poloidal magnetic field-energy is subject to the stability criterion (van Putten & Levinson 2003)

$$\frac{\mathcal{E}_B}{\mathcal{E}_k} < \frac{1}{15}, \quad (5)$$

based on a linear analysis of non-axisymmetric buckling modes. A similar stability analysis for the tilt mode replaces the right hand-side in (5) with  $1/12$ . This upper bound on the magnetic field-strength sets a lower bound on the dissipation rate of black hole-spin energy in the event horizon, and hence a lower bound on the lifetime of rapid spin of the black hole. For the parameters at hand, the lifetime of black hole-spin is hereby tens of seconds (below). The torus itself develops MeV temperatures in a state of suspended accretion (van Putten & Levinson 2003).

### 3.2. Radiatively supernovae powered by black hole-spin energy

The remnant stellar envelope is irradiated from within by high-energy continuum emissions from powerful torus winds, which were released during the preceding GRB. This continuum emission *radiatively* drives a supernova by ejection of the remnant envelope and, when the remnant envelope has expanded sufficiently for its optical depth to this continuum emission has dropped below unity, excites X-ray line-emissions as observed in GRB011211 (Reeves et al. 2001; van Putten 2003). This supernova mechanism is novel in that the supernova-energy derives ab initio from the spin-energy of the black hole, and is otherwise similar but not identical to pulsar driven supernova remnants by vacuum dipole-radiation (Ostriker & Gunn 1971), and magnetorotational driven Type II supernovae by Maxwell stresses (Bisnovatyi-Kogan 1970; LeBlanc & Wilson 1970; Bisnovatyi-Kogan et al. 1976; Wheeler et al. 2000; Akiyama et al. 2003) and associated heating (Kundt 1976).

The energy output in torus winds has been determined in a detailed calculation on the suspended accretion state, and is found to be consistent with the lower bound of Ghisellini

et al. (2002) on the energy in continuum emissions for the line-emissions in GRB011211 (van Putten 2003). In our proposed mechanism for supernovae with X-ray line-emissions, therefore, we envision efficient conversion of the energy output in torus winds into high-energy continuum emissions, possibly associated with strong shocks in the remnant envelope and dissipation of magnetic field-energy into radiation. We note that the latter is a long-standing problem in the pulsars, blazars and GRBs alike (see Levinson & van Putten (1997) and references therein). Conceivably, this process is aided by magnetoturbulence downstream (Layzer 1965; Burbidge 1967). These supernovae will be largely non-spherical, as determined by the collimation radius of the magnetic torus winds, see, e.g., Camenzind (1990) and references therein.

The proposed association of the X-ray line-emissions with the supernova explosion, based on the same underlying large energy in high-energy continuum emissions within the remnant envelope, leads to the prediction that the intensity of line-emissions and the kinetic energy in the ejecta are positively correlated.

### 3.3. Baryon loading in the magnetized baryon-poor jet

A small fraction of the black hole spin energy is channeled along the black hole rotation axis in the form of baryon-poor outflows along an open magnetic flux-tube, as input to the estimated GRB energies  $E_\gamma = 3 \times 10^{50}$  erg of Frail et al. (2001). The baryon content and the loading mechanism of these jets (and essentially of GRB fireballs in any model) is yet an open issue. In one scenario proposed recently (Levinson & Eichler 2003) baryon loading is accomplished through pickup of neutrons diffusing into the initially baryon-free jet from the hot, baryon-rich matter surrounding it. The free neutrons are produced in the hot torus that maintains temperatures of the order of a few MeV, and stream with the baryon-rich wind emanating from the torus to a radius of  $\sim 10^{10}$  cm, above which they recombine with protons to form  $^4\text{He}$ . The pickup process involves a collision avalanche inside the baryon-poor jet (BPJ), owing to the large optical depth for inelastic nuclear collisions contributed by the inwardly diffusing neutrons. The hadronic shower saturates quickly, giving rise to a viscous boundary layer at the outer edge of the BPJ where most of the pickups occur. This boundary layer has a moderate bulk Lorentz factor. The Lorentz factor of the BPJ core, where the baryon density is smaller is much larger initially. The picked-up neutrons in the hot boundary layer can remain free up to a radius of about  $10^{13}$  cm where they recombine, and continue to diffuse into the BPJ core as the BPJ expands. This leads to further collisions in the BPJ core with highly-relativistic baryons coming from below. The total number of picked-up neutrons is estimated to be  $\sim 10^{49.5}$ , although it depends somewhat on the outflow parameters. The

asymptotic bulk Lorentz factor of the BPJ is established in this model at rather large radii ( $\sim 10^{12}$  cm) after neutron pickup is completed, and lies in the range between a few hundreds to a few thousands. The expected variation of the Lorentz factor across the BPJ should give rise to orientation effects that need to be assessed yet. The inelastic nuclear collisions inside the BPJ lead to efficient emission of very high-energy neutrinos (energies well above 1 TeV) with a very hard spectrum. The neutrino fluxes predicted are high enough to be detected by the upcoming  $\text{km}^3$  neutrino detectors, even for a source at a redshift of 1.

#### 4. Timescales and radiation energies

Theoretical predictions in the model of GRBs from rotating black holes can be compared with observations on durations and true GRB energies. We shall do so in dimensionless form, relative to the Newtonian timescale of orbiting matter and the rotational energy of a rapidly rotating Kerr black hole of mass  $7M_\odot$ .

The durations  $T_{90}$  are given by the time of activity of the inner engine of the GRB (Piran & Sari 1998). We propose to identify the lifetime of the inner engine with that timescale  $T_s$  of rapid spin of the black hole. This timescale is effectively set by the rate of dissipation of black hole-spin energy in the event horizon, by spin-down against the surrounding magnetic field of strength

$$B_c \simeq 10^{16} \text{G} \left( \frac{7M_\odot}{M_H} \right) \left( \frac{6M_H}{R} \right)^2 \left( \frac{M_T}{0.03M_H} \right)^{1/2} \quad (6)$$

at the critical value in forementioned stability criterion  $\mathcal{E}_B/\mathcal{E}_k < 1/15$ . We note the increasing observational evidence for super-strong magnetic fields in SGRs and AXPs, see, e.g., Kouveliotou et al. (1999); Thompson & Duncan (2001); Feroci et al. (2001); Ibrahim et al. (2001); Gavril et al. (2002). We then have (van Putten & Levinson 2003)

$$T_s \simeq 90 \text{s} \left( \frac{M_H}{7M_\odot} \right) \left( \frac{\eta}{0.1} \right)^{-8/3} \left( \frac{\mu}{0.03} \right)^{-1/2}. \quad (7)$$

This estimate is consistent with durations of tens of seconds of long gamma-ray bursts (Kouveliotou et al. 1993). This gives rise to the *large* parameter  $\gamma_0 = T_s \Omega_T$ ,

$$\gamma_0 = 1 \times 10^5 \left( \frac{\eta}{0.1} \right)^{-8/3} \left( \frac{\mu}{0.03} \right)^{-1/2} \quad (8)$$

consistent with the observed ratio  $T_{90} \Omega_T \sim 10^5$ .

The true energy in gamma-rays is attributed to baryon-poor energy outflow along an open magnetic flux tube along the axis of rotation of the black hole. As the torus develops

MeV temperatures in the suspended accretion state, it supports a surrounding powerful baryon-rich wind with a mass-loss rate of about  $10^{30} \text{g s}^{-1}$  (van Putten & Levinson 2003). We envision that these torus winds introduce a change in poloidal topology of the inner torus magnetosphere, upon moving the separatrix out to infinity. This creates an open magnetic flux-tube with finite horizon half-opening angle  $\theta_H$ . The open flux-tube forms an artery for a small fraction of black hole-spin energy, releasing magnetized baryon-poor outflows. For a canonical value  $\epsilon \simeq 15\%$  of the efficiency of conversion of kinetic energy-to-gamma rays (for various estimates, see Kobayashi et al. (1997); Daigne & Mochkovitch (1998); Panaitescu & Kumar (2000); Guetta et al. (2001)), we have, based on van Putten & Levinson (2003), a *small* parameter  $\gamma_1 = E_\gamma/E_{rot}$ ,

$$\gamma_1 \simeq \epsilon \theta_H^4. \quad (9)$$

Here, we propose to attribute  $\theta_H$  to poloidal curvature in the inner torus magnetosphere, i.e.,  $\theta_H \simeq M_H/R$  for a magnetic field which is orthogonal to the polar regions of event horizon. This gives  $E_\gamma \simeq 2 \times 10^{50} (\epsilon/0.15)(\eta/0.1)^{8/3} \text{erg}$ , or

$$\gamma_1 \simeq 5 \times 10^{-5} \left( \frac{\epsilon}{0.15} \right) \left( \frac{\eta}{0.1} \right)^{8/3}, \quad (10)$$

consistent with the observed ratio  $E_\gamma/E_{rot} = 7 \times 10^{-5}$  for canonical values of  $M_H = 7M_\odot$  and a rapidly spinning black hole ( $E_{rot} = 0.29M_H$ ).

In the suspended accretion state, the torus emits correlated energies in various channels, namely in gravitational radiation, torus winds and thermal and MeV-neutrino emissions. Their fractional energies, relative to the rotational energy of the black hole, satisfy (van Putten (2003), corrected and simplified)

$$\gamma_2 = \frac{E_{gw}}{E_{rot}} \simeq \frac{\alpha \eta}{\alpha(1+\delta) + f_w^2} \sim \eta, \quad (11)$$

$$\gamma_3 = \frac{E_w}{E_{rot}} \simeq \frac{\eta f_w^2 (1-\delta)^2}{\alpha(1+\delta) + f_w^2} \sim \eta^2, \quad (12)$$

and, the fractional energy dissipated and converted mostly in MeV-neutrino emissions,

$$\gamma_4 = \frac{E_{diss}}{E_{rot}} \sim \delta \eta. \quad (13)$$

The right hand-side gives the asymptotic results in the limit of strong viscosity (large  $\alpha$ ) and small slenderness (small  $\delta$ ), in case of a symmetric flux-distribution described by a fraction  $f_w = 1/2$  of open magnetic flux supported by the torus with connects to infinity. We remark

that the strong viscosity limit satisfies  $\eta \sim 1/(4\alpha)$  in the limit as  $\alpha$  becomes large. These results imply a torus temperature of about 2MeV, whereby the dominant emission is in MeV-neutrino emissions accompanied by subdominant thermal emissions.

The MeV nucleus is relativistically compact, whereby the dominant emission is in gravitational radiation, rather than electromagnetic radiation. Its compactness can be expressed in terms of  $2\pi \int_0^{E_{gw}} f_{gw} dE$ , which expressed the amount of rotational energy relative to the linear size of the system, which is invariant under rescaling of the mass of the black hole according the Kerr metric (Kerr 1963). We have (van Putten (2001); van Putten & Levinson (2002), updated with (13))

$$\gamma_5 = 0.0035 \left( \frac{\eta}{0.1} \right)^2 \quad (14)$$

using the trigonometric expressions  $E_{rot} = 2M_H \sin^2(\lambda/4)$ ,  $\Omega_H = \tan(\lambda/2)/2M_H$  and  $2\pi f_{gw} = 2\Omega_T$ , produced by spin-down of an extreme Kerr black hole with  $\sin \lambda = a/M_H \simeq 1$ , where  $a$  denotes the specific angular momentum. Values  $\gamma_5 > 0.005$  rigorously rule out radiation from a rapidly-spinning neutron star, using the upper bound of 0.005 for their spin-down emissions in gravitational radiation obtained from a Newtonian derivation for a sphere with uniform mass-density.

#### 4.1. A link between gravitational radiation and supernovae energies

The gravitational wave-frequency (1) is constrained by the total kinetic energy in the associated supernova, and the energy requirements for X-ray line-emissions.

The asymptotic fractional energies (13) introduce a relationship between the frequency in quadrupole radiation  $f_{gw}$  and the energy  $E_w$  released in torus-winds, namely

$$f_{gw} \simeq 455 \text{Hz} \left( \frac{E_w}{3.65 \times 10^{52} \text{erg}} \right)^{1/2} \left( \frac{7M_\odot}{M_H} \right)^{3/2}, \quad (15)$$

where the nominal values correspond to  $\eta = 0.1$ . This suggests that we seek observational estimates on  $E_w$  in order to constrain the expected frequency in gravitational radiation. As mentioned in §3, we identify  $E_w$  with the energy  $E_r$  in high-energy continuum radiation which excites the X-ray line-emission in GRB 011211 (Reeves et al. 2001). This points towards

$$E_r \simeq E_w \simeq 4 \times 10^{52} \text{erg}, \quad (16)$$

which is consistent with the required energies for  $E_r$  based on Ghisellini et al. (2002). The kinetic energy  $E_{SN}$  in the supernova ejecta is hereby identified with the radial momentum

imparted by  $E_r$  on the remnant envelope. That is,  $E_{SN} \simeq 0.5\beta E_w$ , whereby

$$E_{SN} \simeq 2 \times 10^{51} \text{erg} \left( \frac{\beta}{0.1} \right) \left( \frac{M_H}{7M_\odot} \right) \left( \frac{\eta}{0.1} \right)^2 \quad (17)$$

with  $\beta = v_{ej}/c$  denoting the velocity  $v_{ej}$  of the ejecta relative to the velocity of light,  $c$ . In the expected aspherical geometry,  $\beta$  refers to a mass-average of the angular distribution of the ejecta. The canonical value  $\beta = 0.1$  refers to the observed velocity of the ejecta in GRB011211. We emphasize that  $E_{SN}$  refers to the true kinetic energy in the ejecta. Eventually, the expanding remnant envelope becomes optically thin, at which stage it may show X-ray line-emissions excited by the underlying continuum emission  $E_r$ .

In (16), we envision efficient conversion of the energy output in torus winds into high-energy continuum emissions, possibly augmented by strong shocks in the remnant envelope and dissipation of magnetic field-energy into radiation. The magnetic field-strength (6) indicates the existence of a transition radius beyond which the magnetic field strength becomes sub-critical. While this transition may bring about a change in the spectrum of radiation accompanying the torus wind, it is unlikely to affect conversion of wind energy to high-energy emissions at larger distances. The reader is referred to Thompson & Duncan (1995) and Duncan (2000) for radiative processes in super-strong magnetic fields.

We note a recent application (Eikenberry & van Putten 2003) of the suspended accretion state at keV temperatures to explain Type B relativistic jet events in the galactic microquasar GRS 1915+105 (Mirabel & Rodríguez 1994). We find qualitatively and quantitatively agreement with observations in energetics, timescales and spectral evolution, including agreement with a spectrally smooth long-duration (400-700 s) hard-dip state. This provides indirect support, albeit at different temperatures and densities, for well-defined, conceivably quasi-periodic frequencies (15).

#### 4.2. GRB980425/SN1998bw and GRB030329/SN2002dh

In our model, *all* emissions are driven by the spin-energy of the central black hole, and hence *all* ejecta are expected to be non-spherical.

The supernova explosion is non-spherical, because the explosion energy (17) represents a fraction of black hole-spin energy which is catalyzed by the surrounding torus (see §3.2).  $E_{SN}$  in (17) is therefore distinct from and generally smaller than the observed isotropic equivalent kinetic energy  $E_{k,iso}$  in the ejecta. Indeed, our canonical value for  $E_{SN}$  agrees remarkably well with the estimated explosion energy of  $2 \times 10^{51}$  erg in SN1998bw (Höflich et al. 1999), based on asphericity in the anomalous expansion velocities of the ejecta. This estimate is



consistent with the partial explosion energy of about  $10^{50}$  erg in ejecta with velocities in excess of  $0.5c$ , where  $c$  denotes the velocity of light (Li & Chevalier 1999). Conversely,  $E_{k,iso}$  can readily assume anomalously large values in excess of  $10^{52}$  erg, depending on the degree of asphericity.

In our model, the explosion energies (17) represent normal SNe Ic values (Höflich et al. 1999). The term “hypernova” (Paczynski 1998) applies only to the apparent energy  $E_{k,iso} \simeq 2 - 3 \times 10^{52}$  erg in GRB980425 (Iwamoto 1998; Woosley et al. 1999) upon assuming spherical geometry, not to the true kinetic energy  $E_{SN}$  in the actual aspherical explosion.

As pointed out in §2, the GRB emissions are strongly anisotropic, produced by beamed baryon-poor jets along the rotational axis of the black hole. Based on consistency between the true GRB event rate, based on (Frail et al. 2001; van Putten & Regimbau 2003), and GRB980425, we further infer that these beamed emissions are accompanied by extremely weak gamma-ray emissions over wide angles or perhaps over all directions. The beaming factor of the baryon poor jet is about 450 (Frail et al. 2001; van Putten & Regimbau 2003). Evidently, the degree of anisotropy in the GRB emissions exceeds the axis ratio of 2 to 3 in the associated supernova ejecta (Höflich et al. 1999) by about two orders of magnitude. While viewing the source on-axis gives rise to the brightest GRB and the largest  $E_{k,iso}$ , we conclude that viewing the source off-axis could give rise to an apparently dim GRB with nevertheless large  $E_{k,iso}$ . This may explain the apparent discrepancy between the dim GRB980425 in the presence of a large  $E_{k,iso}$ , yet normal  $E_{SN}$  (Höflich et al. (1999), Eqn. 17 above), in SN1998bw.

The remarkable similarity between the optical light-curve of SN2003dh associated with GRB030329 (Stanek et al. 2003) supports the notion that GRBs are driven by standard inner engines. GRB030329 was a bright event in view of its proximity, though appeared with a slightly sub-energetic  $E_{\gamma,iso}$ . We attribute this to viewing strongly anisotropic GRB emissions slightly off the rotational axis of the black hole. Based on spectral data, Kawabata et al. (2003) note that the energy  $E_{k,iso}$  of SN2003dh is probably between that of SNe1997ef (e.g. Nomoto et al. (2001); Branch et al. (2001)) and SN1998bw, although SN2003dh and SN1998bw feature similar initial expansion velocities. If SN2003dh allows a detailed aspherical model similar to that of SN1998bw, we predict that the true kinetic energy  $E_{SN}$  will attain a normal value.

The observational constraint  $E_{SNR} \simeq 2 \times 10^{51}$  erg on SN1998bw (Höflich et al. 1999) and consistency with the energy requirement in high-energy continuum emissions for the X-ray line-emissions in GRB011211, therefore, suggest an expectation value of  $f_{gw} \simeq 500\text{Hz}$  according to (15) and (17). It would be of interest to refine this estimate by calorimetry on a sample of SNRs which are remnants of GRBs. Given the true GRB event of about

1 per year within a distance of 100Mpc, we anticipate about 1 GRB-SNR within 10Mpc. These remnants will contain a black hole in a binary with an optical companion, possible representing a soft X-ray transient.

## 5. Line-broadening from Lense-Thirring precession

Quadrupole emissions in gravitational radiation emitted by the torus, possibly accompanied by emissions from higher-order multipole mass-moments, represent a line, which changes on the secular timescale of the change in black hole-spin. This line will broaden, when the torus precesses. Lense-Thirring precession (Lense & Thirring 1918; Wilkins 1972) describes the effect of frame-dragging on a torus whose angular velocity vector is misaligned with the spin-axis of the black hole. Lense-Thirring precession is well-known in a different context, as a possible mechanism for QPOs in X-ray binaries (Stella 1999) as well as in black hole-neutron star binaries (Apostolatos et al. 1994). A torus which is misaligned with the spin-axis of the black hole precesses with essentially the frame-dragging angular velocity described by the Kerr metric. This is accompanied by precession of the black hole, by conservation of angular momentum. Quite generally, the angular momentum of the torus is much less than that of the black hole, whereby the wobbling angle of the black hole is relatively small and can be neglected.

Precession of the orientation of the torus modulates its cosine with the line-of-sight. The observed strain-amplitudes are hereby phase-modulated. Phase-modulation of gravitational radiation from an intrinsic quadrupole moment introduces line-broadening. For small phase-modulations, this is manifest in phase-coherent side-bands, which are separated from twice the orbital frequency by the frequency of Lense-Thirring precession. The origin of a misaligned torus may result from misaligned spin-up of the progenitor star, prior to core-collapse, when the progenitor star is itself misaligned with the orbital plane of the binary.

In Boyer-Lindquist coordinates, we have to leading order the Lense-Thirring angular frequency  $\Omega_{LT} \simeq 2J_H/R^3$  for a black hole angular momentum  $J_H = M^2 \sin \lambda$  in terms of the mass  $M$  and the specific angular momentum  $\sin \lambda = a/M$ . Given the angular velocity  $\Omega_H = \tan(\lambda/2)/2M$  of the black hole and the angular velocity  $\Omega_T \simeq M^{1/2}R^{-3/2}$  of the torus, we have

$$\frac{\Omega_{LT}}{\Omega_H} \simeq 2 \times 10^{-2} \left( \frac{\eta}{0.1} \right)^2 \sin^2(\lambda/2) \quad (18)$$

in terms of the ratio  $\eta = \Omega_T/\Omega_H$  of the angular velocities of the torus to that of the black hole. We expect nominal values  $\eta \sim 0.1$  (van Putten & Levinson 2003), so that  $\Omega_{LT}$  is about

10% of  $\Omega_T$ , or, equivalently, about 1% of  $\Omega_H$ .

An intrinsic mass-inhomogeneity  $m$  in a torus introduces a luminosity of gravitational radiation according to  $L_{gw} = (32/5)(M/R)^5(m/M)^2$ , where  $\mathcal{M} \simeq M(m/M)^{3/5}$  denotes the chirp mass. The gravitational radiation thus produced is anisotropic. For each of the two polarizations, we have

$$h_+ = \frac{4}{r} \frac{1 + \cos^2 \iota}{2} \cos(2\Omega_T t), \quad h_\times = -\frac{4}{r} \cos \iota \sin(2\Omega_T t) \quad (19)$$

where  $\iota$  denotes the angle between the angular momentum and the the line-of-sight. Precession of the torus introduces a time-varying angle  $\iota$ , which modulates the strain amplitudes  $h_+$  and  $h_-$  at the observer. Given a mean angle  $\iota_0$  of the angular momentum of the torus to the line-of-sight and a wobbling angle  $\theta$ , the time-dependent angle  $\iota(t)$  of the same satisfies

$$\cos \iota(t) = \sin \iota_0 \sin \theta \cos(\omega_{LT} t) + \cos \iota_0 \cos \theta. \quad (20)$$

Substitution of  $\cos \iota(t)$  into (19) produces phase-modulation. Fig. 4 illustrates the resulting observed strain-amplitudes for various values of  $\iota_0$ . We may linearize phase-modulation in the case of  $\theta \ll \iota_0$ , whereby  $h_+ = h_+^{(0)} + \theta h_+^{(1)} + O(\theta^2)$ ,  $h_\times = h_\times^{(0)} + \theta h_\times^{(1)} + O(\theta^2)$ , where  $h_+^{(0)} = h_+(\iota_0)$  and  $h_\times^{(0)} = h_\times(\iota_0)$  refer to the strain-amplitudes (19) with  $\iota = \iota_0$ ,

$$h_+^{(1)} = -\frac{\sin(2\iota_0)}{r} [\cos(2\Omega_T + \Omega_{LT}) + \cos(2\Omega_T - \Omega_{LT})] \quad (21)$$

and

$$h_\times^{(1)} = \frac{2 \sin(\iota_0)}{r} [\sin(2\Omega_T + \Omega_{LT}) + \sin(2\Omega_T - \Omega_{LT})]. \quad (22)$$

The ratio of the line-strengths of the side-bands to that of the carrier at  $2\Omega_T$  in terms of the ratio of the respective strain-amplitudes satisfies

$$K \simeq \theta \left( \frac{1 + \cos^2 \iota_0}{1 + 6 \cos^2 \iota_0 + \cos^4 \iota_0} \right)^{1/2} \sin \iota_0, \quad (23)$$

where we used  $\Omega_{LT} \ll 2\Omega_T$ . Averaged over all angles  $\iota_0$ , we have  $\bar{K} \simeq \theta/2$ . Thus, a wobbling angle of about  $30^\circ$  typically produces side-bands of relative strength 20% (taking together  $h_+$  and  $h_\times$  in each side-band).

The above shows that Lense-Thirring precession, if present, may introduce line-broadening by up to 5%.

The same precession introduces time-harmonic modulation of the two principal projections of the torus onto the celestial sphere, one at once and one at twice the precession

frequency. The strength of the two low-frequency lines defines the decay time of the misalignment of the torus. These lines are extremely small, in view of their low-frequencies, allowing Lense-Thirring to persist for timescales at least as long as the durations of long GRBs.

## 6. Stochastic background radiation from GRBs

We may calculate the contribution of GRBs from rotating black holes to the stochastic background in gravitational waves, for a distribution which is locked to the star-formation rate. Below is a semi-analytic summation of the sources, similar but not identical to the numerical summation in (Coward et al. 2002), and includes a correction to the amplitudes reported therein.

The spectral energy density  $dE_{gw}/df$  of a single point source is a redshift-independent distribution, in view of Einstein's adiabatic relationship  $E_{gw}/f = \text{const.}$  The observed energy  $E_{gw}(f, z)$  at an observed frequency  $f$  of a source at redshift  $z$  hereby satisfies  $E_{gw}(f, z) = (1+z)^{-1}E_{gw}((1+z)f, 0)$ . Hence, we have  $E'_{gw}(f, z) = E'_{gw}((1+z)f, 0)$  with  $' = d/df$ . At redshift zero, gravitons emitted by a source at redshift  $z$  are distributed over a surface area  $4\pi d_L^2(z)$ , where  $d_L(z)$  denotes the luminosity area. This gives rise to a spectral energy-density, or equivalently, a flux per unit area at the observer, satisfying  $\tilde{F}_s(f, z) = E'_{gw}/4\pi d_L^2(z)$ . Given a star-formation rate  $R_{SF}(z)$  as measured in the local rest frame per unit of comoving volume  $V$  at redshift  $z$ , the GRB event rate  $R$  as seen by the observer satisfies  $dR(z)/dz = \dot{n}_{GRB}(1+z)^{-1}(R_{SF}(z)/R_{SF}(0))(dV/dz)$ , where  $\dot{n}_{GRB}$  denotes the GRB rate-density at  $z = 0$ . The result contributes to the spectral energy density, i.e., flux per unit area to the stochastic background in gravitons by

$$\tilde{F}_B(f) = \dot{n}_{GRB} \int_0^{z_{max}} \frac{E'_{gw} \Sigma(z)}{(1+z)} dz. \quad (24)$$

The quantity  $\Sigma(z) = (1/4\pi d_L^2(z))(R_{SF}(z)/R_{SF}(0))(dV/dz)$  is observable, representing a count-rate per unit of redshift and luminosity surface area (inferred with reference to a set of standard candles). Here,  $d_L(z) = (1+z)r$  in terms of a spherical radius  $r$ . Considering a closed universe of matter and vacuum energy,  $\Omega_M + \Omega_\Lambda = 1$ , we have the transformation rules  $dV/dz = 4\pi r^2/E(z, \Omega_\Lambda)$  and  $R_{SF}(z, \Omega_\Lambda)/E(z, \Omega_\Lambda) = R_{SF}(z, 0)/E(z, 0)$  (Porciani & Madau 2001), where  $E(z, \Omega_\Lambda) = [\Omega_M(1+z)^{3/2} + \Omega_\Lambda]^{1/2}$ . Here, we suppress a dimensionful factor  $c/H_0$  in  $dV/dz$ , where  $c$  is the velocity of light and  $H_0$  the Hubble constant. A cancellation in  $\Sigma(z)$  leaves a model independent expression  $\Sigma(z) = (1+z)^{-2}R_{SF}(z; 0)R_{SF}(0; 0)^{-1}E(z; 0)^{-1}$ ,

reflecting that it is an observable. It follows that

$$\tilde{F}_B(f) = \dot{n}_{GRB} \int_0^{z_{max}} \frac{\mathcal{F}(z; \Omega_\Lambda)}{1+z} E'_{gw}((1+z)f, 0) \frac{dz}{E(z; \Omega_\Lambda)}, \quad (25)$$

where  $\mathcal{F}(z; \Omega_\Lambda)/(1+z) = R_{SF}(z; \Omega_\Lambda)R_{SF}(0; \Omega_\Lambda)^{-1}(1+z)^{-3}$  represents an observed flux (count-rate per unit area) evolved per unit of surface area and time at  $z = 0$ , ab initio proportional to the star-formation rate as measured in the local rest frame of an Einstein-de Sitter universe per unit of comoving volume. The reader is referred to (Ferrari et al. 1999) and (Phinney 2001) for related expressions.

In the present case, we may use the comoving star-formation density (Madau & Pozzetti 2000)  $R_{SF}(z; 0) = 0.16h_{73}U(z)U(5-z)[1 + 660e^{-3.4(1+z)}]^{-1}M_\odot\text{yr}^{-1}\text{Mpc}^{-3}$  with Hubble constant  $h_{73}$  and Heaviside function  $U(\cdot)$ . We shall further use the estimated GRB event rate of  $250 \text{ yr}^{-1}\text{Gpc}^{-3}$ , which includes a beaming factor of 500 (Frail et al. 2001; van Putten & Regimbau 2003).

The expression (25) can be evaluated semi-analytically, by noting that the gravitational wave-emissions are effectively band limited to a relative bandwidth  $B = \Delta f/f_{gw,s}$  on the order of 10% around (1). Substitution  $u = 1+z$  in (25) gives the equivalent integral  $\tilde{F}_B(f) = \dot{n}_{GRB}E_{gw}B^{-1}f_{gw,s}^{-1} \int_{f_{gw,s}/f(1+\xi)}^{f_{gw,s}/f(1-\xi)} D(u)du$ , where  $2\xi = B$  and  $D(1+z) = R_{SF}(z; \text{EdS})R_{SF}^{-1}(0; \text{EdS})(1+z)^{-9/2}$ . To leading order, the result satisfies  $\tilde{F}_B(f) \simeq \dot{n}_{GRB} (E_{gw}/f)D(f_{gw,s}/f) = \dot{n}_{GRB} (E_0/f_0) (f_0/f) (M/M_0) D(f_{gw,s}/f)$  independent of  $B \ll 1$ . Here, we use the scaling relations

$$E_{gw} = E_0 \left( \frac{M}{M_0} \right), \quad f_{gw,s} = f_0 \left( \frac{M_0}{M} \right) \quad (26)$$

where  $M_0 = 7M_\odot$ ,  $E_0 = 0.203M_\odot(\eta/0.1)$  and  $f_0 = 455\text{Hz}(\eta/0.1)$ . Hence, we have  $y = f_{gw,s}/f = f_0M_0/fM$ . The average over a uniform mass-distribution  $[M_1, M_2]$  ( $\Delta M = M_2 - M_1$ ) then satisfies

$$\langle \tilde{F}_B(f) \rangle \simeq \dot{n}_{GRB} \left( \frac{E_0}{f_0} \right) \left( \frac{f_0}{f} \right) \left( \frac{M_0}{\Delta M} \right) \int_{M_1}^{M_2} \left( \frac{f_0}{f} y^{-1} \right) D(y) \left( \frac{f_0}{f} dy^{-1} \right) \quad (27)$$

i.e.,

$$\langle \tilde{F}_B(xf_0) \rangle = \dot{n}_{GRB} \left( \frac{E_0}{f_0} \right) \left( \frac{M_0}{\Delta M} \right) f_B(x), \quad (28)$$

where

$$f_B(x) = x^{-3} \int_{M_0/M_1x}^{M_0/M_0x} y^{-3} D(y) dy, \quad x = f/f_0. \quad (29)$$

The function  $f_B(x) = f_B(x, M_1, M_2)$  displays a broad maximum of order unity, reflecting the cosmological distribution  $z \simeq 0 - 1$ , preceded by a steep rise reflecting the cosmological distribution at high redshift, and followed by a tail  $x^{-2}$  reflecting a broad distribution of mass at  $z \simeq 0$  (Fig. 4 in Coward et al. (2002)). The broad maximum arises because the luminosity factor  $1/d_L^2(z)$  in energy flux effectively cancels against  $dV/dz$  in this region. In contrast, the spectral strain amplitude  $\propto 1/d_L(z)$  is subdominant at low redshift, giving rise to a sharp peak (Fig. 6 in Coward et al. (2002)) produced by the source population at intermediate redshifts  $z \simeq 1$ . Because  $E'_{gw} \propto M_H^2$ , these peaks are dominated by high-mass sources, and, for the spectral strain amplitude, at about one-fourth the characteristic frequency of  $f_0$ .

We may average (28) over a uniform mass-distribution  $[M_1, M_2] = [4, 14]M_\odot$ , assuming that the black hole mass and the angular velocity ratio  $\eta$  of the torus to that of the black are uncorrelated. Using (26), we have, in dimensionful units,

$$\langle \tilde{F}_B(f) \rangle = 7.45 \times 10^{-9} \hat{f}_B(x) \frac{\text{erg}}{\text{s cm}^2 \text{ Hz}} \quad (30)$$

where  $\hat{f}_B(x) = f_B(x)/\max f_B(\cdot)$ . The associated dimensionless strain amplitude  $\sqrt{S_B(f)} = (2G/\pi c^3)^{1/2} f^{-1} F_B^{1/2}(f)$ , where  $G$  denotes Newton's constant, satisfies

$$\sqrt{S_B(f)} = 2.45 \times 10^{-26} \left( \frac{\eta}{0.1} \right)^{-1} \hat{f}_S^{1/2}(x) \text{ Hz}^{-1/2}, \quad (31)$$

where  $\hat{f}_S(x) = f_S(x)/\max f_S(\cdot)$ ,  $f_S(x) = f_B(x)/x^2$ . Likewise, we have for the spectral closure density  $\tilde{\Omega}_B(f) = f \tilde{F}_B(f)/\rho_c c^3$  relative to the closure density  $\rho_c = 3H_0^2/8\pi G$

$$\tilde{\Omega}_B(f) = 6.11 \times 10^{-9} \left( \frac{\eta}{0.1} \right) \hat{f}_\Omega(x), \quad (32)$$

where  $\hat{f}_\Omega = f_\Omega(x)/\max f_\Omega(\cdot)$ ,  $f_\Omega(x) = x f_B(x)$ . This shows a simple scaling relation for the extremal value of the spectral closure density in its dependency on the model parameter  $\eta$ . The location of the maximum scales inversely with  $f_0$ , in view of  $x = f/f_0$ . The spectral closure density hereby becomes completely determined by the SFR, the fractional GRB rate thereof,  $\eta$ , and the black hole-mass distribution. Fig. 5 shows the various distributions. The extremal value of  $\Omega_B(f)$  is in the neighborhood of the location of maximal sensitivity of LIGO and Virgo (see Fig. 6).

## 7. Dimensionless characteristic strain amplitudes

The strain-amplitude for a band-limited signal is commonly expressed in terms of the dimensionless characteristic strain-amplitude of its Fourier transform. For a signal with

small relative bandwidth  $B \ll 1$ , we have (adapted from Flannagan & Hughes (1998))

$$h_{\text{char}} = \frac{1+z}{\pi d_L(z)} \left( \frac{2E_{gw}}{f_{gw,s}B} \right)^{1/2}, \quad (33)$$

which may be re-expressed as

$$h_{\text{char}} = 6.55 \times 10^{-21} \left( \frac{M}{7M_\odot} \right) \left( \frac{100\text{Mpc}}{d_L} \right) \left( \frac{0.1}{B} \right)^{1/2}, \quad (34)$$

upon ignoring dependence on redshift  $z$ . Note that  $h_{\text{char}}$  is independent of  $\eta$ . The signal-to-noise ratio as an expectation value over random orientation of the source is

$$\left( \frac{S}{N} \right)^2 = \int \left( \frac{h_{\text{char}}}{h_n} \right)^2 d \ln f \simeq \left( \frac{h_{\text{char}}}{h_{\text{rms}}} \right)^2 \frac{B}{5}, \quad (35)$$

where  $h_n = h_{\text{rms}}/\sqrt{5}$ , and  $h_{\text{rms}} = \sqrt{f S_h(f)}$  in terms of the spectral noise-energy density  $S_h(f)$  of the detector. The factor  $1/5$  refers to averaging over all orientations of the source (Flannagan & Hughes 1998). In light of the band-limited signal at hand, we shall consider a plot of

$$h_{\text{char}} \sqrt{B/5} \quad (36)$$

versus  $f_{gw,s}$  according to the dependence on black hole-mass given in (26), using a canonical value  $\eta = 0.1$ . The instantaneous spectral strain-amplitude  $h$  follows by dividing  $h_{\text{char}}$  by the square root of the number of  $2\pi$ -wave periods  $N \simeq f_{gw,s} T_{90} \simeq 2\gamma_0$  according to (8). It follows that

$$h = 3 \times 10^{-23} \left( \frac{0.1}{B} \right)^{1/2} \left( \frac{\eta}{0.1} \right)^{4/3} \left( \frac{\mu}{0.03} \right)^{1/4} \left( \frac{M}{7M_\odot} \right) \left( \frac{100\text{Mpc}}{d_L} \right). \quad (37)$$

## 8. Signal-to-noise ratios

GRBs from rotating black holes produce emissions in the shot-noise region of LIGO and VIRGO, where the noise strain-energy density satisfies  $S_h^{1/2}(f) \propto f$ . We will discuss the signal-to-noise ratios in various techniques. We discuss matched filtering as a theoretical upper bound on the achievable signal-to-noise ratios. We discuss the signal-to-noise ratios in correlating two detectors both for searches for burst sources and for searches for the stochastic background in gravitational radiation.

The S/N-ratio of detections using matched filtering with accurate wave-form templates is given by the ratio of strain amplitudes of the signal to that of the detector noise. Including

averaging over all orientations of the source, we have (Flannagan & Hughes 1998; Cutler & Thorne 2002)

$$\left(\frac{S}{N}\right)_{mf} = \frac{(1+z)\sqrt{2E_{gw}}}{\pi d_L(z)f^{1/2}h_n}. \quad (38)$$

Here, we may neglect the redshift for distances on the order of 100Mpc. Consequently, for matched filtering this gives

$$\left(\frac{S}{N}\right)_{mf} \simeq 8 \left(\frac{S_h^{1/2}(500\text{Hz})}{5.7 \times 10^{-24}\text{Hz}^{-1/2}}\right)^{-1} \left(\frac{\eta}{0.1}\right)^{-3/2} \left(\frac{M}{7M_\odot}\right)^{5/2} \left(\frac{d}{100\text{Mpc}}\right)^{-1}. \quad (39)$$

The expression (39) shows a strong dependence on black hole-mass. For a uniformly distributed mass-distribution, the we have the expectation value  $\overline{S/N} = 18$  for an average over the black hole-mass distribution  $M_H = 4 - 14 \times M_\odot$  as observed in galactic soft X-ray transients; we have  $\overline{S/N} = 7$  for a narrower mass-distribution  $M_H = 5 - 8 \times M_\odot$ . The cumulative event rate for the resulting strain-limited sample satisfies  $\dot{N}(S/N > s) \propto s^{-3}$ .

The signal-to-noise ratio (39) in matched filtering is of great theoretical significance, in defining an upper bound in single-detector operations. Fig. 6 shows the characteristic strain-amplitude of the gravitational wave-signals produced by GRBs from rotating black holes, for a range  $M = 4 - 14 \times M_\odot$  of black hole masses and a range  $\eta = 0.1 - 0.15$  in the ratio of the angular velocities of the torus to the black hole. The ratio of the characteristic strain-amplitude of a particular event to the strain-noise amplitude of the detector (at the same frequency) represents the signal-to-noise ratio in matched filtering. We have included the design sensitivity curves of initial LIGO and Virgo, and Advanced LIGO and Cryogenic Virgo. The Virgo sensitivity curve is a current evaluation, to be validated in the coming months, during the commissioning phase of Virgo.

Evidently, matched filtering requires detailed knowledge of the wave-form through accurate source modeling. The magnetohydrodynamical evolution of the torus in the suspended accretion state has some uncertainties, such as the accompanying accretion flow onto the torus from an extended disk. These uncertainties may become apparent in the gravitational wave-spectrum over long durations. (Similar uncertainties apply to models for gravitational radiation in accretion flows.) For this reason, it becomes of interest to consider methods which circumvent the need for exact wave-forms. In the following, we shall consider detection methods based on the correlation of two detectors, such as the colocated pair in Hanford, or correlation between two of the three LIGO and Virgo sites.

As mentioned in §1, the gravitational wave-spectrum is expected to be band-limited to within 10% of (1), corresponding to spin-down of a rapidly black hole during conversion of



50% of its spin-energy. We may exploit this by correlating two detectors in narrow-band mode – a model-independent procedure that circumvents the need for creating wave-templates in matched filtering. An optimal choice of the central frequency in narrow-band mode is given by the expectation value of (1) in the ensemble of GRBs from rotating black holes.

This optimal choice corresponds to the most likely value of  $M_H$  and  $\eta$  in our model. As indicated, present estimates indicate an optimal frequency within 0.5 to 1kHz. (A good expectation value awaits calorimetry on GRB associated supernova remnants.) A single burst produces a spectral closure density  $\Omega_s$ , satisfying  $T_{90}\Omega_s = 2E'_{gw}f_{gw}/3H_0^2d^2$  in geometrical units. The signal-to-noise ratio obtained in correlating two detector signals over an integration period  $T$  satisfies (Allen & Romano 1999)

$$\left(\frac{S}{N}\right)^2 = \frac{9H_0^4}{50\pi^4} T \int_0^\infty \frac{\Omega_s^2(f)df}{f^6 S_{n1}(f)S_{n2}(f)}. \quad (40)$$

This may be integrated over the bandwidth  $\Delta f_{gw} \ll f_{gw}$ , whereby

$$\left(\frac{S}{N}\right) \simeq \frac{1}{\sqrt{2}} \left(\frac{1}{BN}\right)^{1/2} \left(\frac{S}{N}\right)_{mf}^2 \quad (41)$$

where  $1/BN < 1$  by the frequency-time uncertainty relation. The number of periods  $N$  of frequency  $f_{gw}$  during the burst of duration  $T_{90}$  satisfies  $N \simeq 2T_{90}/P \simeq 4 \times 10^4 \eta_{0.1}^{-8/3} \mu_{0.03}^{-1/2}$ . Hence, we have  $1/BN \sim 10^{-3}$ . Following (39) and (40), we find

$$\left(\frac{S}{N}\right) \simeq 12 f_4^{D1} f_4^{D2} \left(\frac{S_h^{1/2}(500\text{Hz})}{5.7 \times 10^{-24}\text{Hz}^{-1/2}}\right)_{\text{D1}}^{-1} \left(\frac{S_h^{1/2}(500\text{Hz})}{5.7 \times 10^{-24}\text{Hz}^{-1/2}}\right)_{\text{D2}}^{-1} \eta_{0.1}^{-5/3} M_7^5 d_8^{-2} B_{0.1}^{-1/2} \mu_{0.03}^{1/4}, \quad (42)$$

where  $\eta_{0.1} = \eta/0.1$ ,  $M_7 = M/7M_\odot$ ,  $d_8 = d/100\text{Mpc}$ ,  $B_{0.1} = B/0.1$  and  $\mu_{0.03} = \mu/0.03$ , and the factors  $f_4^{Di} = f^{Di}/4$  refer to enhancement in sensitivity in narrow-band mode, relative to broad-band mode. The cumulative event rate for the resulting flux-limited sample satisfies  $\dot{N}(S/N > s) \propto s^{-3/2}$ .

The S/N-ratios of (39) and (42) may be used to derive upper bounds on black hole masses in GRBs, by defining a “no-detection” to correspond to a signal-to-noise ratio of 3 (or less). This is illustrated in Fig. 7.

Given the proximity of the extremal value of  $\Omega_B(f)$  in (32) and the location of maximal sensitivity of LIGO and Virgo, we consider correlating two colocated detectors for searches for the contribution of GRBs to the stochastic background in gravitational waves. According to (40) and (32) for a uniform mass-distribution  $M_H = 4 \times 14M_\odot$ , correlation of the two advanced detectors at LIGO-Hanford gives

$$\left(\frac{S}{N}\right)_B \simeq 5 \left(\frac{S_h^{1/2}(500\text{Hz})}{5.7 \times 10^{-24}\text{Hz}^{-1/2}}\right)_{\text{H1}}^{-1} \left(\frac{S_h^{1/2}(500\text{Hz})}{5.7 \times 10^{-24}\text{Hz}^{-1/2}}\right)_{\text{H2}}^{-1} \eta_{0.1}^{-7/2} T_{\text{1yr}}^{1/2}. \quad (43)$$

Here, the coefficient reduces to 2.2 for a mass-distribution  $M_H = 5 - 8M_\odot$ . The estimate (43) reveals an appreciable dependence on  $\eta$ .

## 9. A detection algorithm for time-frequency trajectories

The proposed gravitational wave-emissions produced by GRBs from rotating black holes are characterized by emission lines which evolve slowly in time. In this two-timing behavior, the Newtonian timescale  $T_K$  on the order of milliseconds serves as the short timescale, and the timescale  $T_s$  of evolution of black hole-spin on the order of tens of seconds serves as the long timescale. In order to circumvent exact wave-form analysis, consider Fourier transforms on an intermediate timescale during which the spectrum is approximately monochromatic. Furthermore, as mentioned in the previous section, we may consider applying correlation techniques. In what follows, we consider the output of the two colocated Hanford detectors, with output

$$s_i(t) = h(t) + n_i(t) \quad (i = 1, 2), \quad (44)$$

where  $h(t)$  denotes the strain amplitude of the source at the detector and  $n_i(t)$  the strain-noise amplitude of H1 and H2.

We may take advantage of the two distinct timescales involved, by considering the time-evolution of the spectrum evaluated over the intermediate timescale  $\tau$ , satisfying  $T_K \ll \tau \ll T_s$ . We may choose  $\tau$  as follows. Consider the phase  $\Phi(t) = \omega t + (1/2)\epsilon\omega t^2$  of a line of slowly-varying frequency  $\dot{\Phi}(t) = \omega(1 + (1/2)\epsilon t)$ , where  $B = \epsilon T_s \simeq 0.1$  denotes the change in frequency over the duration  $T_s$  of the burst. For a duration  $\tau$ , this phase evolution is essentially that of a stationary frequency, provided that  $(1/2)\omega\epsilon\tau^2 \ll 2\pi$ , or

$$\tau/T_s \ll \sqrt{2/BN} \simeq 1/30. \quad (45)$$

For example, a typical burst duration of one minute may be divided into  $N = 120$  sub-windows of 0.5s, each representing about 250 wave-periods at a frequency of 500Hz.

Consider the discrete evolution of the spectrum of the signal of duration  $T_s$  of the burst over  $N$  sub-windows  $I_n = [(n-1)\tau, n\tau]$ , by taking successive Fourier transforms of the  $s_i(t)$  over each  $I_n$ . The two spectra  $\tilde{s}_i(m, n)$ , where  $m$  denotes the  $m$ -th Fourier coefficient, can be correlated according to

$$c(m, n) = \tilde{s}_1(m, n)\tilde{s}_2^*(m, n) + \tilde{s}_1^*(m, n)\tilde{s}_2(m, n). \quad (46)$$

The signal  $h(t)$  contributes to a correlation between the  $s_i(t)$ , and hence to non-negative values  $c_{mn}$ . In general, the presence of noise introduces values of  $c_{mn}$  which are both positive

and negative. Negative values of  $c_{mn}$  only appear in response to (uncorrelated) noise. A plot of positive values  $c_{mn}$ , therefore, will display the evolution of the spectrum of the signal. For example, we may plot all values of  $c_{mn}$  which are greater than a certain positive number, e.g., those for which  $c_{mn} > 0.3 \times \max_{mn} c_{mn}$ . This results are illustrated in Fig. 8.

The TFT algorithm may also be applied to a single detector, i.e., LIGO at Livingston and Virgo at Pisa, provided that the intermediate timescale (45) is much larger than the auto-correlation time in each of the detectors. LIGO and Virgo detectors have sample frequencies of 16kHz and 20kHz. This provides the opportunity for down-sampling a detector signal  $s(t)$  into two separate and interlaced sequences  $s_1(t_i)$  and  $s_2(t'_i)$  ( $t'_i = t_i + \Delta t$ ) that sample  $f_{gw} \simeq 500\text{Hz}$ , while remaining sufficiently separated for the noise between them to be uncorrelated. The coefficients (45) would then be formed out of the Fourier coefficients  $s_1(m, n)$  and  $e^{im\Delta t} s_2(m, n)$ .

The TFT-algorithm is of intermediate order, partly first-order in light of the Fourier transform, and partly second-order in light of the correlation between the Fourier coefficients of the two detector signals. Consequently, its detection sensitivity is between matched filtering and direct correlation in the time-domain, as discussed in the previous section. The gain in signal-to-noise ratio obtained in taking Fourier transforms over sub-windows may circumvent the need for narrow-band operation, allowing use of the two Hanford detectors in their current broad-band configuration.

Application of the TFT algorithm to searches for the contribution of GRBs to the stochastic background radiation could be pursued by taking the sum of the coefficients (46) over successive windows of the typical burst duration, in light of the GRB duty cycle of about one (Coward et al. 2002). The contributions of the signals from distant event add linearly, but are distributed over a broad range of frequencies around 250Hz. A further summation over all sub-windows of 0.5s would result in a net sum over  $10^6$  coefficients during a one-year observational period. The result should be an anomalous broad bump in the noise around 250Hz with a signal-to-noise ratio of order unity, assuming advanced detector sensitivity.

## 10. Conclusions

We consider signal-to-noise ratios for emissions in gravitational radiation for GRB-SNe from rotating black holes. Our model predicts GRBs to be powerful burst sources for LIGO and Virgo in the frequency range above a few hundred Hz, described by the scaling relations (1), and the “big blue bar” in Fig. 6. Based on a true-to-observed GRB event rate ratio of about 450 (Frail et al. 2001; van Putten & Regimbau 2003), the true event rate is estimated

to be one per year within a distance of 100Mpc. Collectively, these events contribute a spectral energy-density  $\Omega_B \simeq 6 \times 10^{-9}$  to the stochastic background in gravitational waves, which peaks around 250Hz.

Our model predicts timescales and energetics in GRBs and provides a new mechanism for the associated supernovae (Table 2). The model predictions are based on first principles and some assumptions, such as an ordered magnetic field in the torus and a successful creation of an open, collimated magnetic flux-tube subtended by the event horizon of the black hole. The predicted durations of about 90 s (see  $\gamma_0$ ), radiation energies of about  $2 \times 10^{50}$  erg from two-sided jets (see  $\gamma_1$ ), and kinetic energies  $2 \times 10^{51}$  erg in non-spherical ejecta (see  $\gamma_3$ ), are in excellent agreement with the observed durations of tens of seconds (Kouveliotou et al. 1993), energies  $E_\gamma \simeq 3 \times 10^{51}$  erg in gamma-rays (Frail et al. 2001), and inferred kinetic energy  $2 \times 10^{51}$  erg in SN1998bw with aspherical geometry (Höflich et al. 1999). The proposed radiation driven ejection process, derived from torus wind energies, is consistent with the energy requirement for X-ray line-emissions in GRB011211. This observational agreement imposes three constraints on the model in good agreement with canonical values ( $M_H \sim 7M_\odot, \eta \sim 0.1, \mu \sim 0.03$ ), thereby obviating the need for any fine-tuning. We are not aware of other models for GRB inner engines which provide similar qualitative and quantitative agreement with a broad range of GRB-SNe phenomenology.

Our model predicts an output in gravitational radiation of about  $4 \times 10^{53}$  erg (see  $\gamma_2$ ) that surpasses  $E_\gamma$  by three orders of magnitude and exceeds the output in any other channel of emissions, including the associated SN and MeV-neutrino emissions. This may be contrasted with Type Ia SNe, whose primary output is a few times  $10^{53}$  erg in neutrinos.

We have calculated the signal-to-noise ratios for the gravitational wave-emissions with fractional energies  $\gamma_2$  in various detection methods. Estimates are presented for matched filtering, as well as narrow- and broad-band correlation techniques for nearby point sources. For the contribution of GRBs to the stochastic background radiation in gravitational waves, estimates are given for broad-band correlation between two colocated detectors.

For nearby point sources, matched filtering provides a theoretical upper bound in detector sensitivity using a single-detector (which can be in broad- or narrow-band mode). We propose to exploit the predicted narrow-band emissions by correlating two detectors in narrow-band mode, to circumvent the need for exact wave-forms in matched filtering. In either case, the position on the sky can be determined using time-of-arrival analysis at three of the LIGO and Virgo interferometers at different locations. Recall further that enhanced sensitivity in narrow-band mode enhances the detection rate considerably, by increase in sensitivity volume beyond the loss of event rates due to frequency selection. Burst sources may also be searched for using the proposed TFT-algorithm, whose sensitivity is interme-

diate between matched filtering and time-domain correlation techniques. This technique takes advantage of the anticipated secular timescale in the evolution of the line-frequencies, and may be used in the correlation of two detectors in broad-band mode. The stochastic background radiation from GRBs can be searched for by correlation between the two colocated LIGO detectors at Hanford. Direct correlation in the time-domain gives an expected  $S/N=5$  in broad-band mode over a one-year integration period. Conceivably, correlation in the Fourier domain allows an improved performance. We note that, after instrumental line-removal, spurious correlations between the two Hanford detectors are considered less likely in the high-frequency range than in the low frequency range.

At current LIGO sensitivity, we may derive upper bounds to black hole-masses in nearby GRB events, by defining a no-detection to correspond to a signal-to-noise ratio of less than 3 in either matched filtering or correlating two detectors in broad- or narrow-band mode. If performed, this procedure would allow an upper bound of about  $150M_{\odot}$  to be put on the mass of the black hole in GRB030229, at current LIGO Hanford sensitivity levels in broad-band mode. We note that published bounds on strain-amplitudes from burst events based on bar detectors apply only to the very highest frequencies predicted by our model. Furthermore, the range of sensitivity implied by these limits corresponds to volume with negligible GRB event rates (given the estimated true GRB rate of 1 per year within 100Mpc).

The burst in gravitational radiation is expected to be contemporaneous with the GRB emissions, extending from the time-of-onset of the GRB, or earlier on the time-scale of seconds during which the baryon-poor outflows punched through the remnant stellar envelope (Woosley et al. 1999), to the end of the GRB. Nearby GRBs are conceivably observable through their weak wide-angle emissions, similar to GRB980425 (Eichler & Levinson 1999). Up to days thereafter, there may appear as radio supernova, representing the ejection of the remnant stellar envelope by the magnetic torus winds. Months thereafter, wide-angle radio afterglows may appear (Levinson et al. 2002; Paczynski 2001). Ultimately, these events leave a supernova remnant surrounding a black hole in a binary with an optical companion (van Putten & Levinson 2003), which may appear as a soft X-ray transient in the scenario of Brown et al. (2000). Thus, long GRBs provide a unique opportunity for integrating LIGO and Virgo detections with current astronomical observations.

There has been a long-standing interest in gravitational wave-burst detections coincident with GRBs (Finn, Mohanty & Romano 1999; Modestino & Moleti 2002). If GRB emissions are conical, then coincident GRB-GWB events are unlikely even with Advanced LIGO sensitivity, since the typical distances of observed GRBs are then a factor of about 8 further away than their unseen counterparts. In this event, we should search for events which are non-coincident with GRBs. However, there is increasing belief that GRB emis-

sions are not conical. Instead, their emissions may be geometrically standard with strong anisotropy (Rossi et al. 2002; Zhang & Meszaros 2002), which includes extremely weak emissions extending over wide-angles (Eichler & Levinson 1999; van Putten & Regimbau 2003). If so, GRB980425/SN1998bw is not anomalous, and we may search for coincidences with such apparently weak GRBs. At the same time, we may consider searches for the associated supernova, using upcoming all-sky surveys such as Pan-STARRS (Kudritzki 2003). The prediction of very similar time-of-onset of the burst in gravitational radiation, weak wide-angle GRB emissions and a radio supernova provides an important observational test for our model.

Detection of the accompanying supernova allows us to determine the distance to the source, and hence the energy emitted by a nearby GRB in gravitational radiation. This predicted energy output gives rise to a relativistic compactness parameter  $\gamma_5 \simeq 2\pi E_{gw} f_{gw}$ , which is predicted to be about  $3 \times 10^{-3}(\eta/0.1)^2$  in units of  $c^5/G$ . A sufficiently high value rigorously rules out rapidly rotating neutron stars. Ultimately, detection of the proposed source of gravitational radiation provides a method for identifying Kerr black holes in the Universe, and for determining their mass-range in GRBs.

**Acknowledgments.** The authors express their thanks for constructive comments from the anonymous referee, the MIT-LIGO Laboratory, A. Brillet, D. Coward, R. Burman, C. Cutler, D. Shoemaker, R. Weiss, P. Fritchel, S. Marka, R. Araya-Gochez, L.S. Finn, R. Frey, P. Höflich and G. Tee. This work is supported by Grant No. R01-1999-00020 from the Korean Science and Engineering Foundation, and by the LIGO Observatories, constructed by Caltech and MIT with funding from NSF under cooperative agreement PHY 9210038. The LIGO Laboratory operates under cooperative agreement PHY-0107417. This paper has been assigned LIGO document number LIGO-P030041-00-D.

## REFERENCES

- Abramovici, A., et al., 1992, *Science*, 292, 325
- Allen, B., Romano, J.D., 1999, *Phys. Rev. D.*, 59, 102001
- Antonelli, L.A., Piro, L., Vietri, M., et al., 2000, *ApJ*, 545, L39
- Apostolatos, T.A., Cutler, C., Sussman, G.J., Thorne, K.S., 1994, *Phys. Rev. D*, 49, 6274
- Astone, P., et al., 2002, *PRD*, 2002, 66, 102002
- Bisnovatyi-Kogan, G.S., 1970, *Astron. Zh.*, 47, 813

- Bisnovatyi-Kogan, G.S., Popov, Yu. P., & Samochin, A.A., 1976, *Ap & S.S.*, 41, 287
- Bonnell, I.A., & Pringle, J.E., 1995, *MNRAS*, 273, L12
- Bradaschia, C., et al., 1992, *Phys. Lett., A*, 163, 15
- Branch, D., et al., 2001, in *SNe and GRBs*, eds. M. Livio, N. Panagia and K. Sahu (Cambridge University Press), 144
- Brown, G.E., et al., 2000, *NewA*, 1
- Burbidge, E.M., 1967, *ARRA*, 5, 399
- Camenzind, M., 1990, *Rev. Modern Astron.*, 3, 234
- Cappellaro, E., Turatto, M., Tsvetkov, D.Yu., Bartunov, O.S., Pollas, C., Evans, R., & Hamuy, M., 1997, *A&A*, 322, 431
- Carter, B., 1968, *Phys. Rev.*, 174, 1559
- Chevalier, R.A., & Li, Z.-Y., *ApJ*, 520, L29
- Chu, Y.-H., Kim, S., Points, S.D., Petre, R., & Snowden, S.L., 2000, *ApJ*, 119, 2242
- Coburn, W., & Boggs, S.E., 2003, *Nature*, 423, 415
- Coward, D.M., van Putten, M.H.P.M., & Burman, R.R., 2002, *ApJ*, 580, 1024
- Cutler, C., & Thorne, K.S., 2002, *in*, *Proc. GR16*, Durban, South Afrika
- Daigne, F., & Mochkovitch, R., 1998, *MNRAS*, 296, 275
- Davies, M.B., King, A., Rosswog, S., & Wynn G., 2002, *ApJ*, 579, L63
- Duncan, R.C., 2000, *astro-ph/0002442*
- Eichler, D., & Levinson, A., 1999, *ApJ*, 521, L117
- Eichner, D., & Levinson, A., *ApJ Lett.*, to appear
- Eikenberry, S., & van Putten, M.H.P.M., 2003, *ApJ*, submitted
- Feroci, M., Hurley, K., Duncan, R.C., & Thompson, C., 2001, *ApJ*, 549, 1021
- Ferrari, V., Matarrese, S., & Schneider, R., 1999, *MNRAS*, 303, 258
- Ferrari, V., Miniutti, G., & Pons, J.A., 2003, *MNRAS*, submitted; *astro-ph/0210581(v2)*

- Finn, L.S., Mohanty, S.D., Romano, J.D., 1999, PRD, 60, 121101
- Flannagan, E., & Hughes, S., 1998, Phys. Rev. D., 57, 4535
- Frail et al., 2001, ApJ, 567, L41
- Fryer, C.L., Holz, D.E., Hughes, S.A., 2002, ApJ, 565, 430
- Fryer, C.L., Woosley, S.E., & Heger, A., 2001, ApJ, 550, 372
- Galama, T.J. et al., 1998, Nature, 395, 670
- Gavriil, F.P., Kaspi, V.M., Woods, P.M., 2002, Nature, 419, 142
- Ghisellini, G., Lazatti, D., Rossi, E., & Rees, M.J., 2002, A&A, 389, L33
- Guetta, D., Spada, M., & Waxman, E., 2001, ApJ, 559, 101
- Hawking, S.W., 1975, Commun. Math. Phys., 43, 1999
- Höflich, P.J., 1991, A&A, 246, 481
- Höflich, P.J., Wheeler, J.C., Wang, L., 1999, ApJ, 521, 179
- Höflich, P.J., Khoklov, A., & Wang, L., 2001, in Proc. Texas Conf. Relat. Astroph., AIP-Publ; astro-ph/0104025
- Hjorth, J., et al., 2003, 423, 847
- Hulse, R.A., & Taylor, J.H., 1975, ApJ, 195, L51
- Ibrahim, A.I., et al., 2001, ApJ, 558, 237
- Iwamoto, K., 1999, ApJ, 512, L47
- Iwamoto, K., et al., 1998, Nature, 395, 672
- Kawabata, K.S., et al., 2003, ApJ, submitted; astro-ph/0306155
- Kardashev, N.S., Astron. Zh., 41, 807; *ibid.*, 1964, Sov. Astron., 8, 643
- Kardashev, N.S., 1995, MNRAS, 276, 515
- Katz, J.I., Canel, L.M., 1996, ApJ, 471, 915
- Kerr, R.P., 1963, Phys. Rev. Lett., 11, 237



- Kobayashi, S., Piran, T., & Sari, R., 1997, *ApJ*, 490, 92
- Kobayashi, S., & Mészáros, P., 2002, *ApJ*, 585, L89
- Kouveliotou, C., et al., 1993, *ApJ*, 413, L101
- Kouveliotou, C., et al., 1999, *ApJ*, 510, L115
- Kudritzki, R., 2003, private commun.; see <http://www.ifa.hawaii.edu/pan-starrs>
- Kulkarni, S.R., 1998, *Nature*, 395, 663
- Kundt, W., 1976, *Nature*, 261, 673
- Layzer, D., 1965, *ApJ*, 141, 837
- Lazzati, D., Ramirez-Ruiz, E., & Rees, M.J., 2002, *ApJ*, 572, L57
- Lazzarini, A., 2003, E-030000-R, <http://www.ligo.caltech.edu>
- LeBlanc, J.M., & Wilson, J.R., 1970, *ApJ*, 161, 541
- Lense, J., and Thirring, H., 1918, *Phy. Z.*, 19, 156
- Levinson, A., & Eichler, D., *Phys. Rev. Lett.*, 83, 236
- Levinson, A., & Eichler, D., *ApJ*, 594, L19
- Levinson, A., & van Putten, M.H.P.M., 1997, *ApJ*, 488, 69
- Levinson, A., Ofek, E., Waxman, E., & Gal-Yam A., 2002, *ApJ*, 567, 923
- Li, Z.-Y., & Chevalier, R., 1999, *ApJ*, 526, 716
- MacFadyen, A., & Woosley, S.E., 1999, *ApJ*, 524, 262
- Madau, P., & Pozzetti, L., 2000, *MNRAS*, 312, L9
- Mönchmeyer, R., Schäfer, G., Müller, E., & Kates, R.E., 1991, *A&A*, 246, 417
- Mineshige, S., Hosokawa, T., Machida, M., & Matsumoto, R., 2002, *PASJ*, 54, 655
- Mészáros, P., 2002, *Ann. Rev. Astron. Astroph.*, 40, 137
- Mirabel, I.F. & Rodríguez, L.F. 1994, *Nature*, 371, 46
- Modestino, G., & Moleti, A., 2002, *PRD*, 65, 022005

- Nakamura, T., & Fukugita, M., 1989, *ApJ*, 337, 466
- Narayan, R. & Piran, T., Shemi, A., 1991, *ApJ*, 379, L17
- Nomoto, K., et al., 2001, in *SNe and GRBs*, eds. M. Livio, N. Panagia and K. Sahu (Cambridge University Press), 144
- Ostriker, J.P., & Gunn, J.E., 1971, *ApJ*, 164, L95
- Paczynski, B.P., 1998, *ApJ*, 494, L45
- Paczynski, B.P., 2001, *Acta Astronomica*, 51, 81
- Panaiteanu, A., & Kumar, P., 2000, *ApJ*, 543, 66
- Papaloizou, & Pringle, 1984, *MNRAS*, 208, 721
- Peters, P.C., & Mathews, J., 1963, *Phys. Rev.*, 131, 435
- Phinney, E.S., 1991, *ApJ*, L17
- Phinney, E.S., 2001, *astro-ph/0108028*
- Piran, T., & Sari, R., 1998, In: Olinto, A.V., Friedman, J.A., Schramm, D.N. (Eds.), *Proc. 18th Texas Symposium on Relativity, Astrophysics and Cosmology*. World Scientific, Singapore, p34.
- Piran, T., 1999, *Phys. Rep.*, 314, 575; *ibid.* 2000, *Phys. Rep.* 333, 529
- Piro, L., Costa, E., Feroci, M., et al., 1999, *ApJ*, 514, L73
- Piro, L., Garmire, G., Garcia, M., et al., 2000, *Science*, 290, 955
- Porciani, C., & Madau, P., 2001, *ApJ*, 548, 522
- Price, P.A., et al., 2003, *Nature*, 423, 844
- Punturo, M., 2003, *Virgo Internal Note VIR-NOT-PER-1390-51*
- van Dyk, S.D., Sramek, R.A., Weiler, K.W., & Panagia, N., 1993, *ApJ*, 409, 162
- Rees, M.J., & Meszaros, P., 1994, *ApJ*, 430, L93
- Reeves, J.N., et al., 2002, *Nature*, 416, 512
- Rossi, E., Lazzati, D., & Rees, M.J., 2002a, *MNRAS*, 332, 945

- Salmonson, J.D., 2001, ApJ, 546, L29
- Schaefer, B.E., Deng, M., & Band, D.L., 2001, ApJ, 563, L123
- Shapiro, S.L., & Teukolsky, S.A., 1983, Black holes, White Dwarfs, and neutron stars. Wiley, New York
- Akiyama, S., Wheeler, J.C., Meier, D.L., Lichtenstadt, I., 2003, ApJ, 584, 954
- Stanek, K.Z., et al., 2003, ApJ, 591, L17
- Stella, L., 1999, in Proceedings of X-ray Astronomy (Bologna, Italy, 6-10 Sept. 1999, AIP conference proceedings vol. 599) eds. N. E. White, G. Malaguti, and G. G.C. Palumbo
- Taylor, J.H., 1994, Rev. Mod. Phys., 66, 711
- Thompson, C., & Duncan, R.C., 1995, MNRAS, 275, 255
- Thompson, C., & Duncan, R.C., 2001, ApJ, 561, 980
- Tricarico, P., et al., 2001, PRD, 63, 082002
- Turatto, M., 2003, in Proc. Supernovae and GRBs, ed. K.W. Weiler; astro-ph/0301107
- Uemura, M., et al., 2003, Nature, 423, 843
- van Putten, M.H.P.M., 1999, Science, 284, 115
- van Putten, M.H.P.M., & Ostriker, E.C., 2001, 552, L31
- van Putten, M.H.P.M., 2000, Phys. Rev. Lett., 84, 3752
- van Putten M.H.P.M., 2001, Phys. Rep., 345, 1
- van Putten, M.H.P.M., 2002, ApJ, 575, L71
- van Putten M.H.P.M., & Levinson, A., 2002, Science, 294, 1837
- van Putten, M.H.P.M., 2003, ApJ, 583, 374
- van Putten M.H.P.M., & Levinson, A., 2003, ApJ, 584, 967
- van Putten M.H.P.M., & Regimbau, T., 2003, ApJ, 593, L15
- van Putten, M.H.P.M., H.K. Lee, C.H. Lee, & H. Kim, 2003, submitted
- Wald, R., 1974, Phys. Rev. D., 10, 1680

- Weiler, K.W., Panagia, N., & Montes, 2001, ApJ, 670
- Wheeler, J.C., Yi, I., Höflich, P., Wang, L., 2000, ApJ, 537, 810
- Wilkins, D., 1972, Phys. Rev. D5, 814
- Willingale, R., Osborne, J.P., O’Brien, P.T., Ward, M.J., Levan, A., & Page, K.L., 2003, MNRAS, submitted; astro-ph/0307561
- Woosley, S., 1993, ApJ, 405, 273
- Woosley, S.E., Eastman, R.G., & Schmidt B.P., 1999, ApJ, 516, 788
- Yoshida, A., Namiki, M., Otani, C., et al., 1999, A&AS, 138, 433
- Zhang, B., & Meszaros, P., 2002, ApJ, 571, 876

Table 1. A sample of 33 GRBs with individually determined redshifts <sup>a</sup>

GRB	Redshift $z$	Photon flux <sup>b</sup>	Luminosity <sup>c</sup>	$\theta_j$ <sup>d</sup>	Instrument
970228	0.695	10	$2.13 \times 10^{58}$		SAX/WFC
970508	0.835	0.97	$3.24 \times 10^{57}$	0.293	SAX/WFC
970828	0.9578	1.5	$7.04 \times 10^{57}$	0.072	RXTE/ASM
971214	3.42	1.96	$2.08 \times 10^{59}$	> 0.056	SAX/WFC
980425	0.0085	0.96	$1.54 \times 10^{53}$		SAX/WFC
980613	1.096	0.5	$3.28 \times 10^{57}$	> 0.127	SAX/WFC
980703	0.966	2.40	$1.15 \times 10^{58}$	0.135	RXTE/ASM
990123	1.6	16.41	$2.74 \times 10^{59}$	0.050	SAX/WFC
990506	1.3	18.56	$1.85 \times 10^{59}$		BAT/PCA
990510	1.619	8.16	$1.40 \times 10^{59}$	0.053	SAX/WFC
990705	0.86			0.054	SAX/WFC
990712	0.434	11.64	$7.97 \times 10^{57}$	> 0.411	SAX/WFC
991208	0.706	11.2*	$2.48 \times 10^{58}$	< 0.079	Uly/KO/NE
991216	1.02	67.5	$3.70 \times 10^{59}$	0.051	BAT/PCA
000131	4.5	1.5*	$3.05 \times 10^{59}$	< 0.047	Uly/KO/NE
000210	0.846	29.9	$1.03 \times 10^{59}$		SAX/WFC
000301C	0.42	1.32*	$8.37 \times 10^{56}$	0.105	ASM/Uly
000214	2.03				SAX/WFC
000418	1.118	3.3*	$2.27 \times 10^{58}$	0.198	Uly/KO/NE
000911	1.058	2.86	$1.72 \times 10^{58}$		Uly/KO/NE
000926	2.066	10*	$3.13 \times 10^{59}$	0.051	Uly/KO/NE
010222	1.477				SAX/WFC
010921	0.45				HE/Uly/SAX
011121	0.36	15.04*	$6.63 \times 10^{57}$		SAX/WFC
011211	2.14				SAX/WFC
020405	0.69	7.52*	$1.58 \times 10^{58}$		Uly/MO/SAX
020813	1.25	9.02*	$8.19 \times 10^{58}$		HETE
021004	2.3				HETE
021211	1.01				HETE
030226	1.98	0.48*	$1.35 \times 10^{58}$		HETE
030323	3.37	0.0048*	$4.91 \times 10^{56}$		HETE
030328	1.52	2.93*	$4.31 \times 10^{58}$		HETE
030329	0.168	0.0009*	$7.03 \times 10^{52}$		HETE

<sup>a</sup>Compiled from S. Barthelmy's IPN redshifts and fluxes (<http://gcn.gsfc.nasa.gov/gcn/>) and J.C. Greiner's catalogue on GRBs localized with WFC (BeppoSax), BATSE/RXTE or ASM/RXTE, IPN, HETE-II or INTEGRAL (<http://www.mpe.mpg.de/jcg/grbgeb.html>)

<sup>b</sup>in  $\text{cm}^{-2}\text{s}^{-1}$

<sup>c</sup>Photon luminosities in  $\text{s}^{-1}$  derived from the measured redshifts and observed gamma-ray fluxes for the cosmological model described in §2

<sup>d</sup>Opening angles  $\theta_j$  in the GRB-emissions refer to the sample listed in Table I of Frail et al.(2001).

\*Extrapolated to the BATSE energy range 50 - 300 keV using the formula given in Appendix B of Sethi et Bhargavi (2001)

Table 2. Model predictions<sup>a</sup> versus observations GRB-SNe

Quantity	Units	Expression	Observation
$E_{gw}$	erg	$4 \times 10^{53} \eta_{0.1} M_{H,7}$	
$f_{gw}$	Hz	$500 \eta_{0.1} M_7^{-1}$	
$\Omega_B$	1	$6 \times 10^{-9} @ 250 \text{Hz}$	
$E_{SN}$	erg	$2 \times 10^{51} \beta_{0.1} \eta_{0.1}^2 M_{H,7}$	$2 \times 10^{51} \text{erg}^b$
$E_\gamma$	erg	$2 \times 10^{50} \epsilon_{0.15} \eta_{0.1}^{8/3} M_{H,7}$	$3 \times 10^{50} \text{erg}^c$
$E_{\gamma \rightarrow X}^d$	erg	$4 \times 10^{52} \bar{\epsilon} \eta_{0.1}^2 M_{H,7}$	$> 4.4 \times 10^{51} \text{erg}^e$
$T_s$	s	$90 \eta_{0.1}^{-8/3} M_{H,7} \mu_{0.03}^{-1/2}$	$T_{90}$ of tens of s <sup>f</sup>
Event rate	yr <sup>-1</sup>		1 within $D = 100 \text{Mpc}^g$

<sup>a</sup>Based on a critical ratio  $\mathcal{E}_B/\mathcal{E}_k \simeq 1/15$  of poloidal magnetic field energy-to-kinetic energy in the torus with ratios  $b/R < 0.3260$  of minor-to-major radius

<sup>b</sup>SN1998bw with aspherical geometry, estimated by Höflich et al.(1999)

<sup>c</sup>True energy in gamma-rays produced along open magnetic flux-tubes; Frail et al.(2001)

<sup>d</sup>Continuum gamma-ray emission produced by torus winds with undetermined efficiency  $\bar{\epsilon}$  as energy input to X-ray line-emissions

<sup>e</sup>Ghisellini et al.(2002)

<sup>f</sup>Kouveliotou et al.(1993)

<sup>g</sup>Local estimate based on Frail et al.(2001) and van Putten & Regimbau et al.(2003)

### Figure captions

**FIGURE 1.** Cartoon of the proposed model for GRB-supernovae from rotating black holes (not to scale): core-collapse in an evolved massive star produces an active MeV-nucleus consisting of a rotating black hole (Woosley 1993; Brown et al. 2000) surrounded by a torus which may be magnetized with the magnetic field of the progenitor star (Paczynski 1998). The torus assumes a state of suspended accretion, wherein it catalyzes black hole-spin energy at an efficiency given by the ratio  $\eta = \Omega_T/\Omega_H$  of the angular velocity  $\Omega_T$  of the torus and  $\Omega_H$  of the black hole. Because the nucleus is relativistically compact, the torus radiates this input predominantly into gravitational radiation, and, to a lesser degree, into magnetic winds and MeV-neutrino emissions. A small fraction of about  $\theta_H^4$  of black hole-spin energy is released in baryon-poor jets along open magnetic flux-tubes along the rotational axis of the black hole, where  $\theta_H$  denotes the half-opening angle on the event horizon. This output serves as input to the GRB-afterglow emissions. As these jets punch through the remnant stellar envelope (MacFadyen & Woosley 1999), the GRB may be delayed by seconds (Woosley et al. 1999), and thereby appear after the onset of gravitational wave-emissions. A radiatively driven supernova appears subsequently in response to high-energy continuum emissions produced by the magnetic torus winds. When the envelope has expanded sufficiently to becoming optically thin, X-ray line-emissions may appear conceivably accompanied by radio emissions.

**FIGURE 2.** Redshift distributions of the flux-limited sample of 33 GRBs with individually determined redshifts, the true-but-unseen sample assuming the GRB event rate is locked to the star-formation rate (hachured), and the sample of detectable GRBs predicted by our model according to a log-normal peak-luminosity distribution function (grey). The continuous line represents the cosmic SFR ( $\Lambda$ -dominated CDM universe). The unseen-to-observed event rate for standard sources with anisotropic emissions is hereby 450. (Reprinted from M.H.P.M. van Putten & T. Regimbau, 2003)

**FIGURE 3.** A causal spin-connection between the torus and the event horizon of the black hole arises by virtue of an inner torus of open magnetic field-lines, equivalent to the connection between pulsars and asymptotic infinity when viewed in poloidal cross-section. These open magnetic field-lines are endowed with Dirichlet-radiative boundary conditions. The inner face of the torus (angular velocity  $\Omega_+$ ) and the black hole (angular velocity  $\Omega_H$ ) herein corresponds to a pulsar surrounded by infinity with relative angular velocity  $\Omega_H - \Omega_+$  (Mach’s principle). It hereby receives energy and angular momentum from the black hole, whenever  $\Omega_H - \Omega_+ > 0$ . The outer face of the torus (angular velocity  $\Omega_-$ ) is equivalent to a pulsar with angular velocity  $\Omega_-$ , and it loses energy and angular momentum by the same equivalence. This spin-connection is established by an approximately uniformly magnetized torus, represented by two counter-oriented current rings, and, for rapidly rotating black

holes, an equilibrium magnetic moment of the horizon. In poloidal topology, the magnetic flux-surfaces are illustrated in the approximation of flat space-time. The dashed line is the separatrix between the flux-surfaces of the inner and the outer magnetospheres. Moving it by a stretch-fold-cut to infinity leaves an open magnetic flux-tube subtended by the event horizon of the black hole (not shown). (Reprinted from M.H.P.M. van Putten & A. Levinson, 2003, ApJ, 584, 937 ©2003 University of Chicago Press)

**FIGURE 4.** The observed strain-amplitudes  $h_+$  and  $h_\times$  are subject to amplitude modulation by varying orientation of the torus relative to the line-of-sight, in response to Lense-Thirring precession. This introduces side-bands about the carrier frequency  $2\Omega_T$ , where  $\Omega_T$  denotes the angular velocity of the torus. These side-bands are separated from the carrier frequency by once (in both  $h_+$  and  $h_\times$ ) and twice (in  $h_+$ ) the Lense-Thirring frequency. Shown are the strain-amplitudes for the case of  $\iota_0 = 0, \pi/8, \pi/4, \pi/2$  for a wobbling angle of  $30^\circ$  and a Lense-Thirring precession frequency of  $1/8$  of the orbital frequency. The amplitude corresponds to a source at unit distance, and the index refers to the number of orbital periods. (Reprinted from M.H.P.M. van Putten, H.K. Lee, C.H. Lee & H. Kim (2003).)

**FIGURE 5.** (*Left*) Shown is the observed flux  $\mathcal{F}(z, \text{EdS})/(1+z)^3$  in gravitational radiation from GRBs as a function of the SFR [ $M_\odot \text{yr}^{-1} \text{Mpc}^{-3}$ ] in an Einstein-de Sitter universe ( $H_0 = 73 \text{km s}^{-1} \text{Mpc}^{-1}$ ), evolved to a per unit of surface area and unit of time at  $z = 0$ . Note the peak at  $z \simeq 1$ . (*Right*) Shown is the spectral flux-density  $\Omega_B(f)$  for a cosmological distribution of GRBs from rotating black holes as burst sources of gravitational radiation assuming a uniform mass distribution in the range of  $M_H = 4 - 14 \times M_\odot$  (top curve) and  $M_H = 5 - 8 \times M_\odot$  (lower curve). The results are shown for  $\eta = 0.1$ . The extremal value of  $\Omega_B(f)$  is in the neighborhood of the location of maximal sensitivity of LIGO and Virgo.

**FIGURE 6.** GRBs from rotating black holes produce a few tenths of  $M_\odot$  in long duration bursts of gravitational radiation (van Putten 2001; van Putten & Levinson 2003). These emissions are parametrized by the black hole mass  $M_H = 4 - 14M_\odot$  and the ratio  $\eta \sim 0.1 - 0.15$  of the angular velocities of the torus and the black hole. The signal is band limited with relative bandwidth  $B \simeq 10\%$ . The dark region shows  $h_{\text{char}} B^{1/2}/\sqrt{5}$  of the orientation-averaged characteristic dimensionless spectral strain-amplitude  $h_{\text{char}}$ . The source distance is  $D = 100 \text{Mpc}$ , corresponding to an event rate of once per year. The dimensionless strain-noise amplitudes  $h_{\text{rms}}(f) = \sqrt{f S_h(f)}$  of Initial/Advanced LIGO (lines), Initial/Cryogenic VIRGO (dashed; Punturo (1999)) are shown with lines removed, including various narrow-band modes of Advanced LIGO (dot-dashed), where  $S_h(f)$  is the spectral energy-density of the dimensionless strain-noise of the detector. Short GRBs from binary black hole-neutron star coalescence may produce similar energies distributed over a broad



bandwidth, ranging from low frequencies during inspiral up to 1kHz during the merger phase.

**FIGURE 7.** Shown are the achievable upper bounds on the mass of the black hole in GRB030329 ( $z = 0.167$ ,  $T_{90} = 25$  s) at current LIGO sensitivity ( $S_h^{1/2} = 4 \times 10^{-22} \text{Hz}^{-1/2}$ ), assuming a no-detection result in applications of matched filtering (solid), in correlating two detectors in narrow-band mode (dot-dashed), and in correlating two detectors in broad-band mode (dotted). The labels refer to signal-to-noise ratios 1, 2 and 3. In broad-band mode, correlation between the two LIGO Hanford detectors at current sensitivity would permit placing an upper bound on the black hole mass in GRB030329 ( $D = 800 \text{Mpc}$ ) of about  $150 M_\odot$ .

**FIGURE 8.** GRBs from rotating black holes are expected to produce line-emissions in gravitational radiation which evolve slowly in time, on the timescale of spin-down of the black hole. This produces trajectories in the temporal evolution of the spectrum of the signal. We may search for these trajectories, by performing Fourier transforms over time-windows of intermediate size, during which the signal is approximately monochromatic. The results shown illustrate a slowly-evolving line-emission for a long burst, partitioned in  $N = 128$  sub-windows of  $M = 256$  data points, in the presence of noise with an instantaneous signal-to-noise ratio of 0.15. The left two windows show the absolute values of the Fourier coefficients, obtained from two simulated detectors with uncorrelated noise. The trajectory of a simulated slowly-evolving emission-line becomes apparent in the correlation between these two spectra (right window). The frequency scales with Fourier index  $i$  according to  $f = (i - 1)/\tau$  ( $i = 1, \dots, M/2 + 1$ ), where  $\tau$  denotes the time-period of the sub-window.

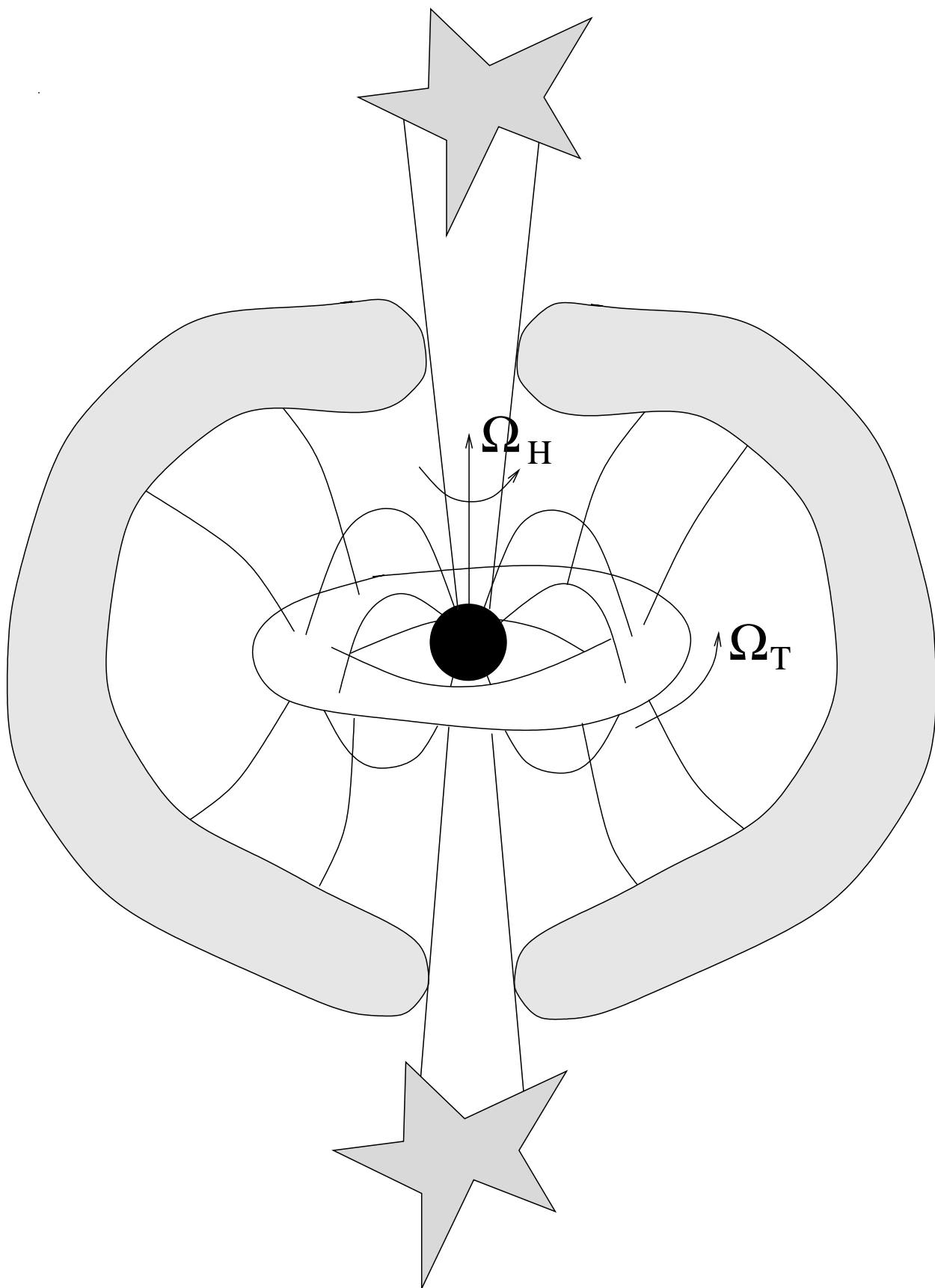


Fig. 1.—

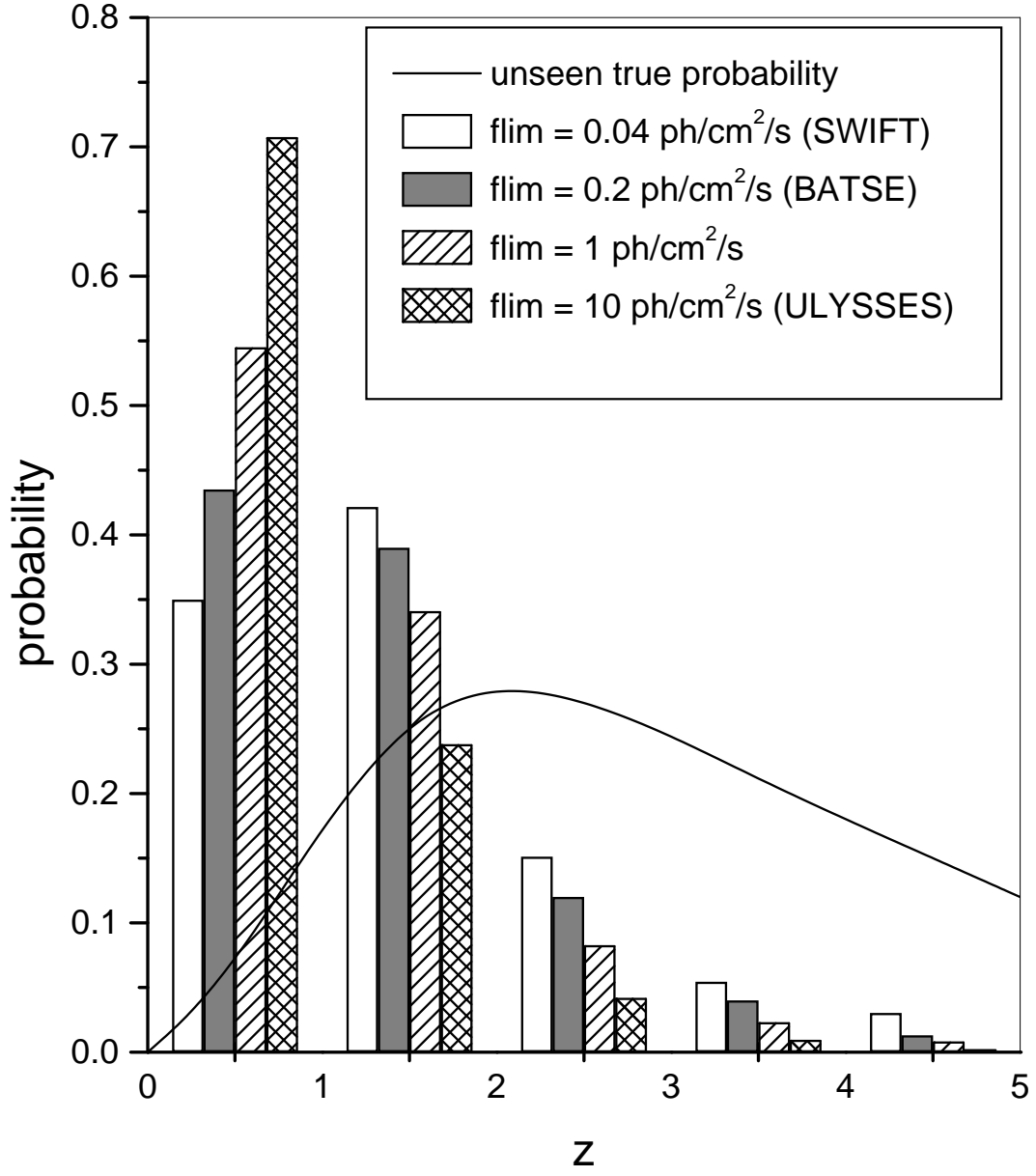


Fig. 2.—

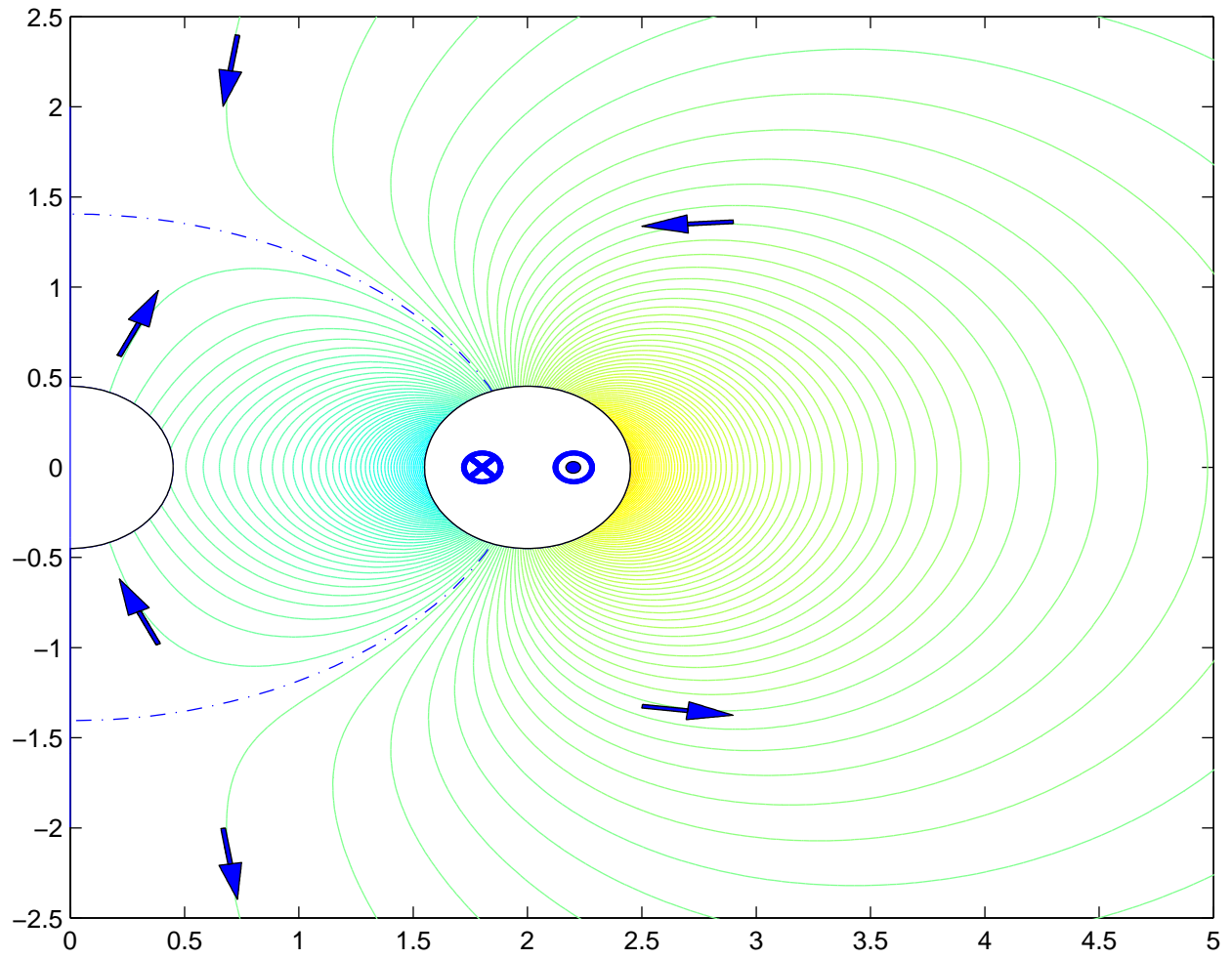


Fig. 3.—

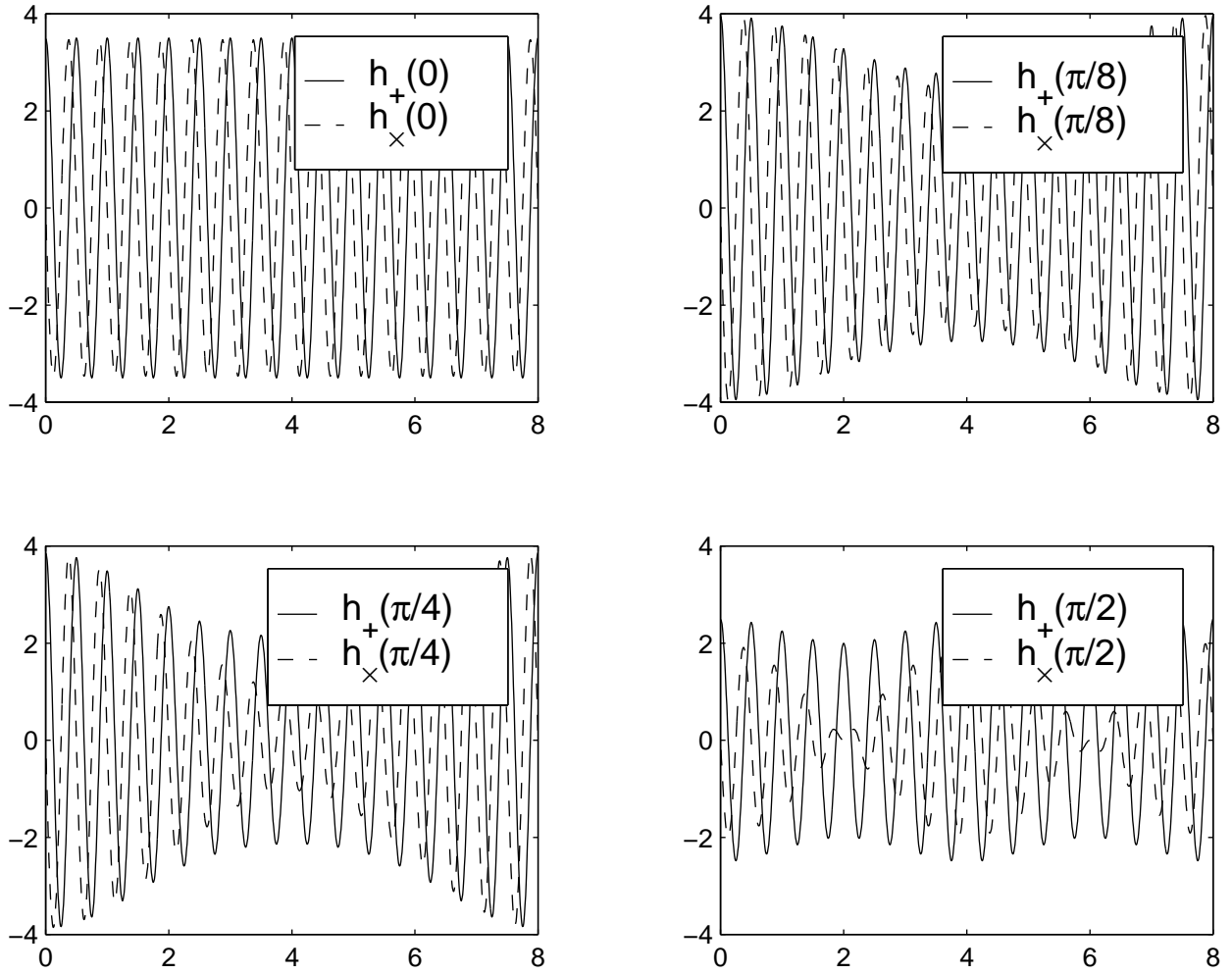


Fig. 4.—

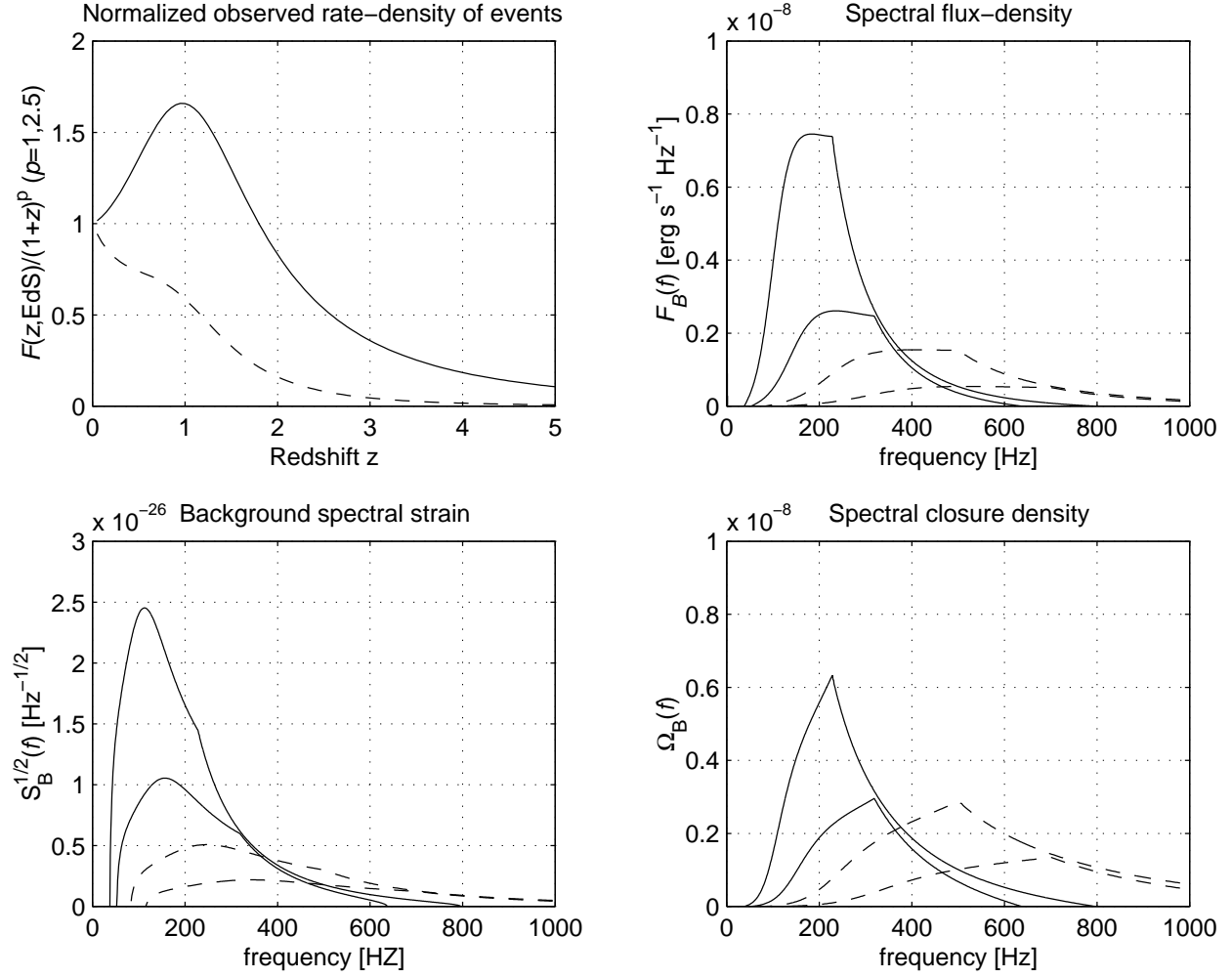


Fig. 5.—

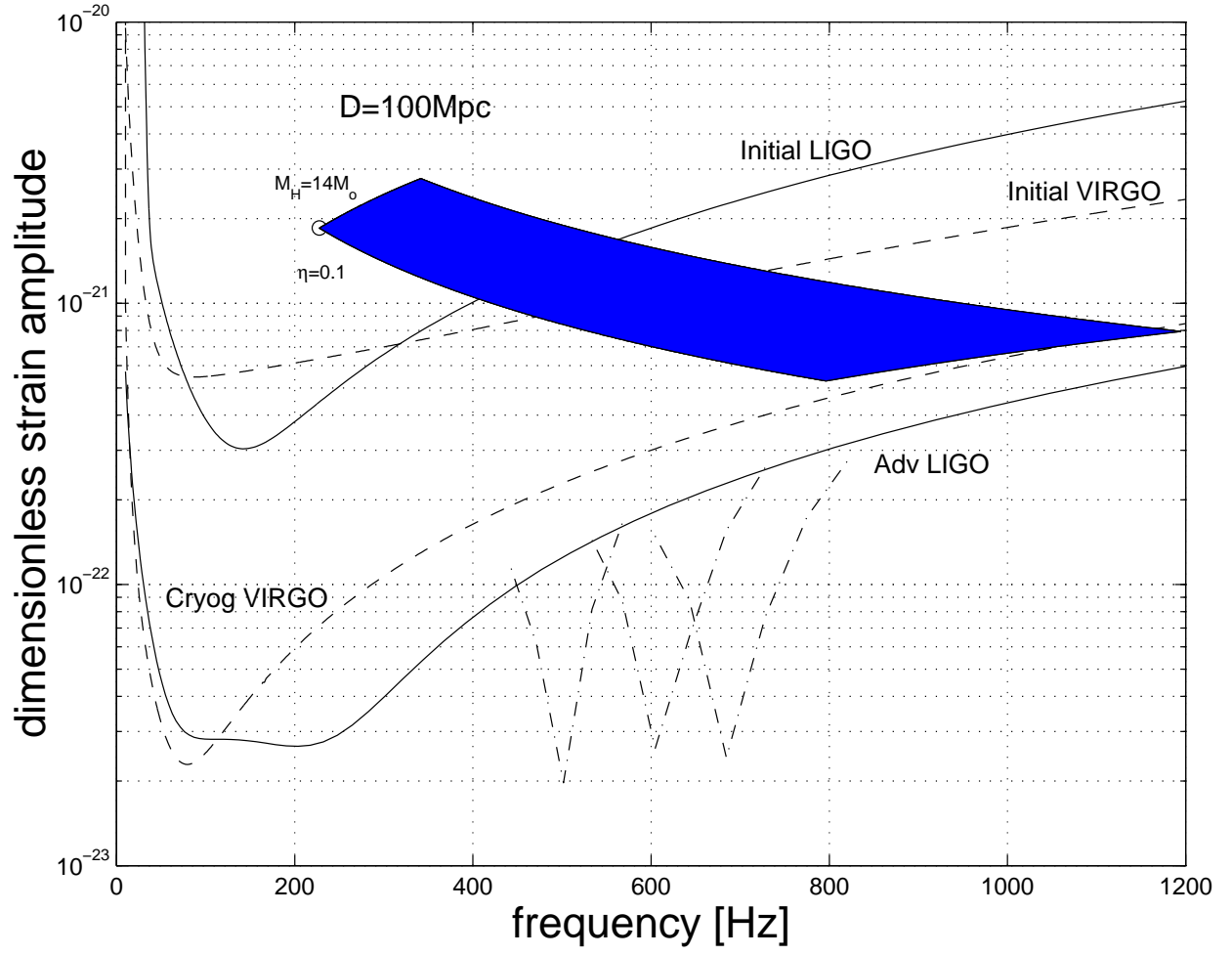


Fig. 6.—

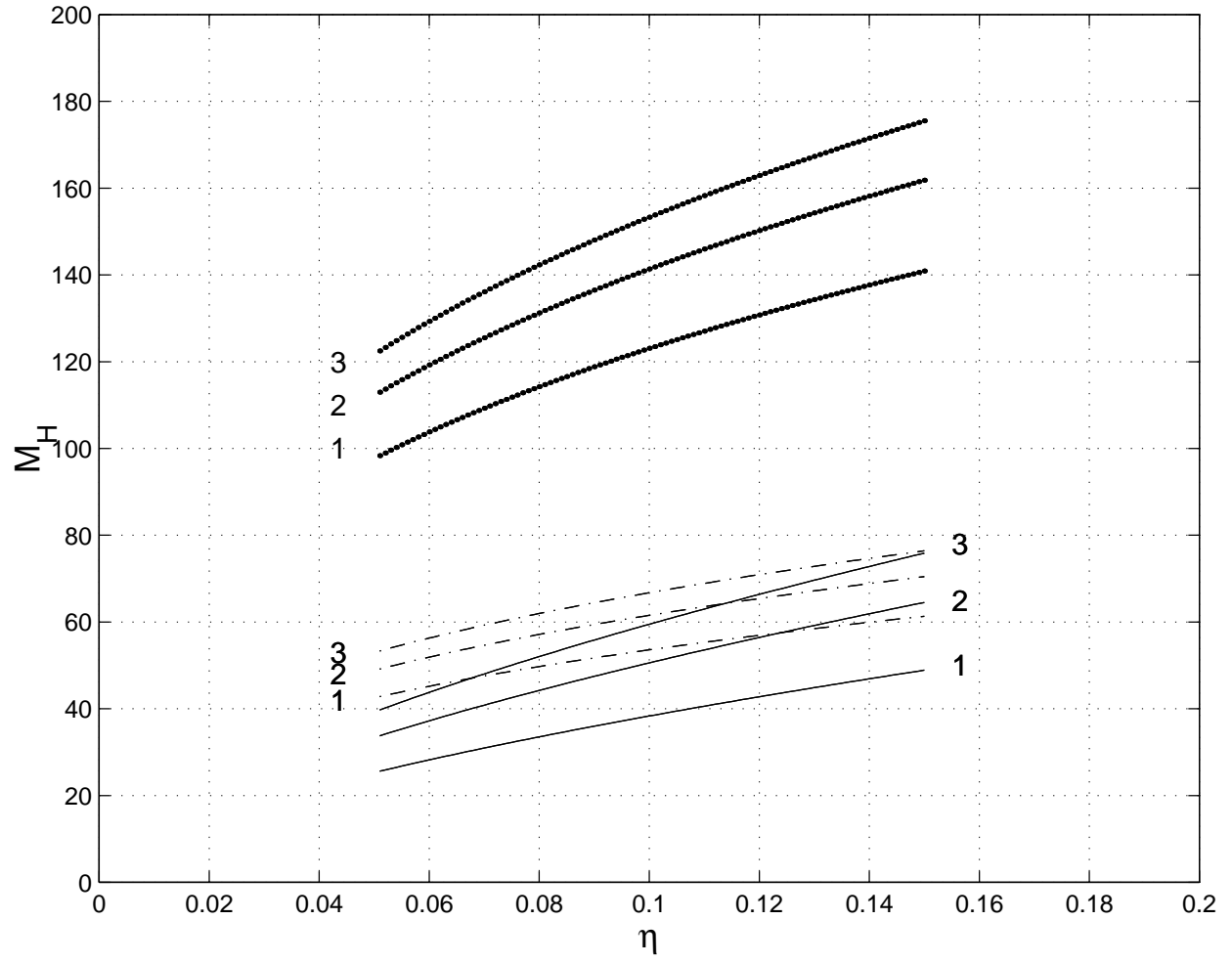


Fig. 7.—



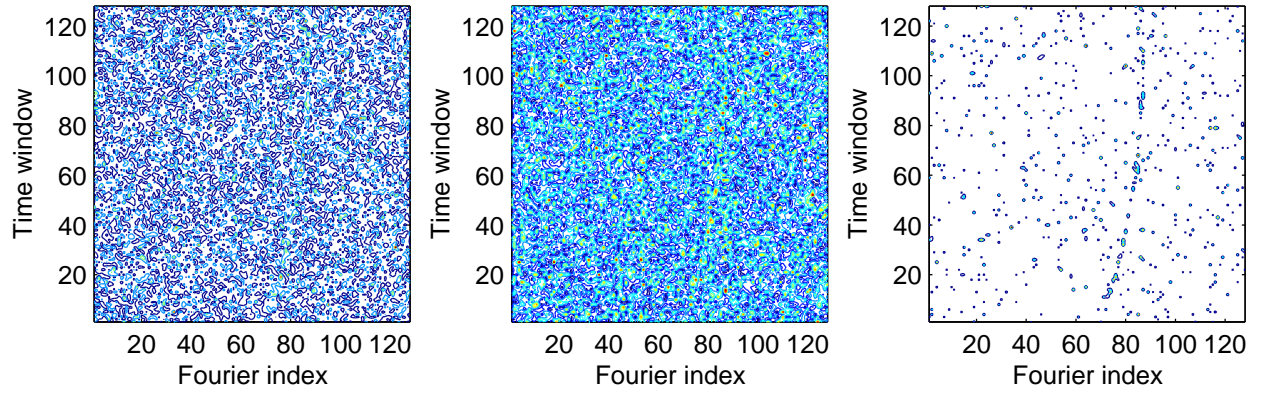


Fig. 8.—